

# The Moon Mineralogy Mapper ( $M^3$ ) imaging spectrometer for lunar science: Instrument description, calibration, on-orbit measurements, science data calibration and on-orbit validation

R. O. Green,<sup>1</sup> C. Pieters,<sup>2</sup> P. Mouroulis,<sup>1</sup> M. Eastwood,<sup>1</sup> J. Boardman,<sup>3</sup> T. Glavich,<sup>1</sup> P. Isaacson,<sup>2</sup> M. Annadurai,<sup>4</sup> S. Besse,<sup>5</sup> D. Barr,<sup>1</sup> B. Buratti,<sup>1</sup> D. Cate,<sup>1</sup> A. Chatterjee,<sup>1</sup> R. Clark,<sup>6</sup> L. Cheek,<sup>2</sup> J. Combe,<sup>7</sup> D. Dhingra,<sup>2</sup> V. Essandoh,<sup>1</sup> S. Geier,<sup>1</sup> J. N. Goswami,<sup>8</sup> R. Green,<sup>1</sup> V. Haemmerle,<sup>1</sup> J. Head,<sup>2</sup> L. Hovland,<sup>1</sup> S. Hyman,<sup>1</sup> R. Klima,<sup>2,9</sup> T. Koch,<sup>1</sup> G. Kramer,<sup>7,10</sup> A. S. K. Kumar,<sup>11</sup> K. Lee,<sup>1</sup> S. Lundein,<sup>1</sup> E. Malaret,<sup>12</sup> T. McCord,<sup>7</sup> S. McLaughlin,<sup>5</sup> J. Mustard,<sup>2</sup> J. Nettles,<sup>2</sup> N. Petro,<sup>13</sup> K. Plourde,<sup>1</sup> C. Rach,<sup>1</sup> J. Rodriguez,<sup>1</sup> C. Runyon,<sup>14</sup> G. Sellar,<sup>1</sup> C. Smith,<sup>15</sup> H. Sobel,<sup>1</sup> M. Staid,<sup>16</sup> J. Sunshine,<sup>5</sup> L. Taylor,<sup>17</sup> K. Thaisen,<sup>17</sup> S. Tompkins,<sup>18</sup> H. Tseng,<sup>1</sup> G. Vane,<sup>1</sup> P. Varanasi,<sup>1</sup> M. White,<sup>1</sup> and D. Wilson<sup>1</sup>

Received 6 January 2011; revised 27 July 2011; accepted 27 July 2011; published 29 October 2011.

[1] The NASA Discovery Moon Mineralogy Mapper imaging spectrometer was selected to pursue a wide range of science objectives requiring measurement of composition at fine spatial scales over the full lunar surface. To pursue these objectives, a broad spectral range imaging spectrometer with high uniformity and high signal-to-noise ratio capable of measuring compositionally diagnostic spectral absorption features from a wide variety of known and possible lunar materials was required. For this purpose the Moon Mineralogy Mapper imaging spectrometer was designed and developed that measures the spectral range from 430 to 3000 nm with 10 nm spectral sampling through a 24 degree field of view with 0.7 milliradian spatial sampling. The instrument has a signal-to-noise ratio of greater than 400 for the specified equatorial reference radiance and greater than 100 for the polar reference radiance. The spectral cross-track uniformity is >90% and spectral instantaneous field-of-view uniformity is >90%. The Moon Mineralogy Mapper was launched on Chandrayaan-1 on the 22nd of October. On the 18th of November 2008 the Moon Mineralogy Mapper was turned on and collected a first light data set within 24 h. During this early checkout period and throughout the mission the spacecraft thermal environment and orbital parameters varied more than expected and placed operational and data quality constraints on the measurements. On the 29th of August 2009, spacecraft communication was lost. Over the course of the flight mission 1542 downlinked data sets were acquired that provide coverage of more than 95% of the lunar surface. An end-to-end science data calibration system was developed and all measurements have been passed through this system and delivered to the Planetary Data System (PDS.NASA.GOV). An extensive effort has been undertaken by the science team to validate the Moon Mineralogy Mapper science measurements in the context of the mission objectives. A focused spectral, radiometric, spatial, and uniformity validation effort has been pursued

<sup>1</sup>Jet Propulsion Laboratory, California Institute of Technology, Pasadena, California, USA.

<sup>2</sup>Department of Geological Sciences, Brown University, Providence, Rhode Island, USA.

<sup>3</sup>Analytical Imaging and Geophysics, LLC, Boulder, Colorado, USA.

<sup>4</sup>ISRO Satellite Center, Bangalore, India.

<sup>5</sup>Astronomy Department, University of Maryland, College Park, Maryland, USA.

<sup>6</sup>U.S. Geological Survey, Denver, Colorado, USA.

<sup>7</sup>Bear Fight Center, Winthrop, Washington, USA.

<sup>8</sup>Physical Research Laboratory, ISRO, Ahmedabad, India.

<sup>9</sup>Now at Planetary Exploration Group, Applied Physics Laboratory, Johns Hopkins University, Laurel, Maryland, USA.

<sup>10</sup>Lunar and Planetary Institute, Houston, Texas, USA.

<sup>11</sup>Space Applications Centre, ISRO, Ahmedabad, India.

<sup>12</sup>Applied Coherent Technologies, Herndon, Virginia, USA.

<sup>13</sup>Planetary Geodynamics Branch, NASA Goddard Space Flight Center, Greenbelt, Maryland, USA.

<sup>14</sup>Department of Geology and Environmental Geosciences, College of Charleston, Charleston, South Carolina, USA.

<sup>15</sup>Spacecraft Systems and Services, ATK, Pasadena, California, USA.

<sup>16</sup>Planetary Science Institute, Tucson, Arizona, USA.

<sup>17</sup>Planetary Geosciences Institute, Department of Earth and Planetary Sciences, University of Tennessee, Knoxville, Tennessee, USA.

<sup>18</sup>DARPA, Arlington, Virginia, USA.

with selected data sets including an Earth-view data set. With this effort an initial validation of the on-orbit performance of the imaging spectrometer has been achieved, including validation of the cross-track spectral uniformity and spectral instantaneous field of view uniformity. The Moon Mineralogy Mapper is the first imaging spectrometer to measure a data set of this kind at the Moon. These calibrated science measurements are being used to address the full set of science goals and objectives for this mission.

**Citation:** Green, R. O., et al. (2011), The Moon Mineralogy Mapper ( $M^3$ ) imaging spectrometer for lunar science: Instrument description, calibration, on-orbit measurements, science data calibration and on-orbit validation, *J. Geophys. Res.*, 116, E00G19, doi:10.1029/2011JE003797.

## 1. Introduction

[2] Spectroscopy has been used for more than a century as a scientific analytical method to investigate composition and to measure and understand processes based upon the interaction of light with matter. It has been used to determine properties at distances ranging from astronomical to microscopic. The capability to analytically determine composition from a remote perspective is a key advantage of spectroscopy. With the development of advanced detectors in the late 20th century, instruments began to be conceived and developed that measured spectra in image format. These imaging spectrometers enabled a new level of scientific measurement and understanding with the delivery of spectroscopically derived composition in full spatial context. This capability was identified as critical to NASA missions of exploration and discovery. For solar system exploration, NASA has developed a number of imaging spectrometers for planetary exploration including the Near Infrared Mapping Spectrometer (NIMS) to Jupiter; the Visual and Infrared Mapping Spectrometer (VIMS) to Saturn; the Deep Impact near infrared imaging spectrometer; and the Compact Reconnaissance Imaging Spectrometers for Mars (CRISM) [Murchie et al., 2007]. Other nations have also recognized the measurement capability of imaging spectrometers for science and exploration, for example VIRTIS on Rosetta [Coradini et al., 1998], OMEGA [Bibring et al., 2005] on Mars Express and HySI [Kumar et al., 2009] also on Chandrayaan-1. In parallel for measurement of the Earth system, imaging spectroscopy has proceeded with the Airborne Imaging Spectrometer (AIS) [Vane et al., 1984], the Airborne Visible/Infrared Imaging Spectrometer [Green et al., 1998], the airborne Mapping Reflected energy Spectrometer (MaRS) [Simi et al., 2009] as well as the Hyperion imaging spectrometer [Ungar et al., 2003; Green et al., 2003]. As exemplified by these science instruments and with the addition of new designs and enabling technologies, imaging spectrometers have advanced as critical remote measurement science instruments with improved measurement characteristics and reduced mass, power, and volume requirements.

[3] In the summer of 2004 Earth's Moon remained an object that had not been measured in a dedicated manner by an imaging spectrometer. Yet, spectroscopic measurements of the returned Apollo lunar samples as well as selected telescope and other observations showed the Moon to be an ideal candidate for detailed mapping by a visible to near infrared imaging spectrometer [e.g., McCord et al., 1981; Pieters, 1986]. In the summer of 2004 a guest instrument opportunity was opened by the Indian Space Resource

Organization (ISRO) for the Chandrayaan-1 mission to the Moon. Chandrayaan-1 was planned as a comprehensive two year, 100 km polar orbiting, global measurement mission [Goswami and Annadurai, 2008]. The guest payload opportunity was nominally limited to instruments weighing less than 10 Kg and requiring less than 10 Watts of power. Based upon this opportunity, a proposal to ISRO for the Moon Mineralogy Mapper ( $M^3$ ) to be included on the Chandrayaan-1 mission was submitted by NASA. After an ISRO review,  $M^3$  was placed on a short list of possible instruments to be included on Chandrayaan-1. In parallel with the proposal to ISRO, a proposal to develop the imaging spectrometer was submitted to the 2004 NASA Discovery Program Mission of Opportunity. The proposed  $M^3$  instrument built upon the more than two decades previous experience in imaging spectrometer development as well as a set of new enabling capabilities.

[4] In February 2005 NASA selected  $M^3$  as a Mission of Opportunity and in March 2005 ISRO confirmed  $M^3$  as a guest instrument on Chandrayaan-1.  $M^3$  was the last instrument selected for the Chandrayan-1 mission that included a spacecraft with twelve distinct instrument payloads [Goswami and Annadurai, 2009]. These Chandrayaan-1 instrument included: the Terrain Mapping Camera (TMC); Lunar Laser Ranging Instrument (LLRI); Hyper Spectral Imager (HySI); High Energy X-ray spectrometer (HEX); Moon Impact Probe (MIP); Chandrayaan-1 X-ray Spectrometer (C1XS); Sub-keV Atom Reflecting Analyzer (SARA); Spectrometer InfraRed (SIR-2), MiniSynthetic Aperture Radar (miniSAR); Radiation Dose Monitor (RADOM); and the Moon Mineralogy Mapper ( $M^3$ ). Figure 1 shows the nominal configuration of the Chandrayaan-1 spacecraft with  $M^3$  mounted on the anti-sun side panel. The proposed  $M^3$  science imaging spectrometer was designed to map the entire surface of the Moon for the first time with complete visible to near infrared imaging spectroscopy at fine spatial resolution.

## 2. Science Measurement Approach and Characteristics

[5] The  $M^3$  Discovery opportunity mission was proposed within the context of NASA's strategic planning in 2004. As such,  $M^3$  was proposed with both a high level science and a high level exploration goal that were supported by a set of refined and traceable objectives. The science goal was to characterize and map the lunar surface composition in the context of its geologic evolution. The exploration goal was to assess and map the Moon's mineral resources at high spatial resolution, 70 m sampling, to support planning for

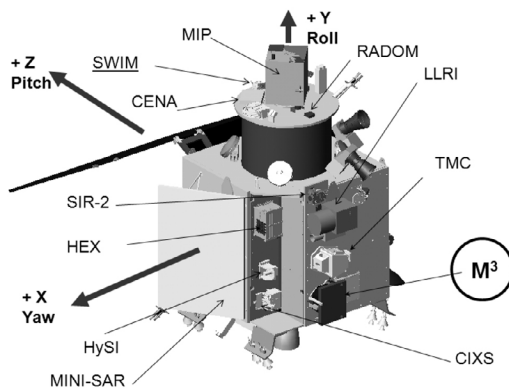


**Figure 1.** The baseline configuration of the Chandrayaan-1 spacecraft with the location of the M<sup>3</sup> imaging spectrometer with optical, radiator, and electronics subsystems depicted on the anti-sun side of the spacecraft. The aperture points toward the Moon in the +X direction and the cross-track field of view in the XZ plane. Twelve total instruments are included in the Chandrayaan-1 payload.

future, targeted missions. To pursue these goals a set of seven objectives were identified: (1) characterize the lunar highland rocks in the context of geologic processes; (2) identify and characterize the diversity of lunar volcanism; (3) identify and map the presence of hydrous phases; (4) identify the recent impact flux at 1 AU and use craters as probes to the interior; (5) identify areas of rare or previously unseen lunar materials; (6) determine if detected polar Hydrogen is related to H<sub>2</sub>O; and (7) identify and map areas with diverse “feedstock” for future utilization. This suite of goals and objectives are directly addressable with an accurate map of the surface composition of the Moon.

[6] The goals and objectives of M<sup>3</sup> are well suited to surface mineral and compositional mapping via spectroscopy in the visible and near-infrared portion of the electromagnetic spectrum [Hunt and Salisbury, 1970; Pieters, 1993; Clark, 1999]. Figure 2 shows an example set of laboratory measured reflectance spectra of lunar minerals and soils returned by the Apollo program measured in the Reflectance Experiment Laboratory (RELAB) [Pieters, 1983] over the M<sup>3</sup> spectral range. The diagnostic spectral absorption features of these materials provide the scientific basis for mapping the composition of the lunar surface with an imaging spectrometer. This spectral range is also appropriate for passive reflected energy spectroscopy with illumination of the lunar surface provided by the Sun at ~1 AU. Additional measurable signal arises at longer wavelengths from thermal emitted energy when the lunar surface temperature is near 300 K and above. To achieve the science goals and objectives of M<sup>3</sup>, measurement of the full spectral range with contiguous sampling is required. This reflected light spectroscopic measurement approach is best suited to conditions of small zenith angle solar illumination when the reflected signal is strong and there are few shadows. Measurement of the full spectral shape allows minerals and other components to be unambiguously identified and abundances estimated even in the presence of compositional mixtures. In addition, this broad range

spectroscopic approach enables discovery of previously undetected lunar surface materials.

[7] Inclusion as a guest instrument on the Chandrayaan-1 mission established a set of strict observational constraints on the M<sup>3</sup> spectroscopic science measurement approach. First among these was the baseline inertially fixed polar orbit with a nominal altitude of 100 ± 20 km and 32 km orbit-to-orbit spacing. From this orbit and altitude the solar zenith angle at the equator shifts by 1° per day during a set of 12 orbits. Over the nominal 2 year mission this orbit offered four well-illuminated observation periods of three months each with the equatorial solar zenith angle between 0° and 30°. Additional constraints from the Chandrayaan-1 mission included mass, power, volume, and especially downlink transmission capacity from lunar orbit to Earth receiving stations. Mapping the Moon efficiently with contiguous coverage using the four limited observation periods at the appropriate spatial scale required selection of a high efficiency pushbroom type imaging spectrometer with a field-of-view (FOV) of 24°. Details of the science measurement mapping strategy and implementation are described by *Boardman et al.* [2011].

[8] Beginning from the imaging spectroscopy science measurement approach and including the Chandrayaan-1 mission constraints, a refined set of science measurement requirements were established. These requirements established the spectral, radiometric, spatial, and uniformity properties of the imaging spectrometer science measurement. Table 1 provides the key science measurement requirements for the M<sup>3</sup> imaging spectrometer on Chandrayaan-1. The most critical of these was specification of a broad spectral range between 430 and 3000 nm with 10 nm sampling to optimally capture the spectral diversity of the expected materials on the lunar surface. The spectral range was specifically extended to 3000 nm to offer the capability to detect the possible presence of minor quantities of hydrated compounds adjacent to the permanently shadowed cold trap craters in the polar regions of the Moon. This broad spectral

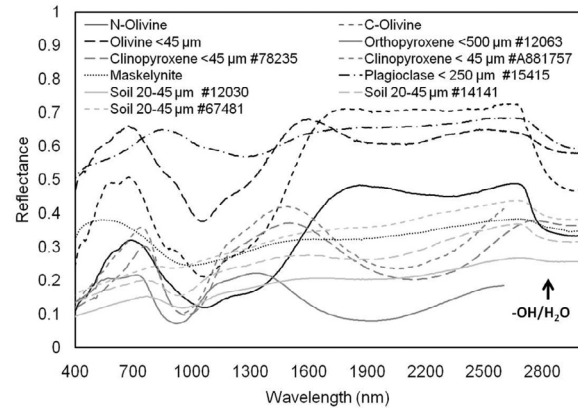


**Figure 2.** Laboratory measured reflectance spectra of Moon minerals and soils showing the diversity of spectral signatures present in the spectral range from 400 to 3000 nm in the visible through near infrared portions of the spectrum. The strong absorption feature near 2900 nm has been assumed to be caused by adsorbed hydroxyl/water from the Earth’s atmosphere.

**Table 1.** Key Science Measurements' Requirements of the M<sup>3</sup> Imaging Spectrometer to Address the Mission Goals and Objectives<sup>a</sup>

	Requirements
<i>Spectral</i>	
Range	430 ± 50 to 3000 ± 50 nm
Sampling	10 ± 0.2 nm constant
Response	FWHM* < 1.5 X sampling
Accuracy	≤1 nm
<i>Radiometric</i>	
Range	0 to specified saturation
Sampling	12 bits measured
Accuracy	≥90% (<10% uncertainty)
Precision (SNR)	≥400 at equatorial reference radiance ≥100 at polar reference radiance
<i>Spatial</i>	
Range	24 ± 2° field-of-view
Sampling	0.7 ± 0.07 milliradian
Response	FWHM* < 1.5 X sampling
<i>Uniformity</i>	
Spectral-cross-track	≥90% uniformity of spectral position over the field-of-view
Spectral-IFOV	≥90% uniformity of IFOV variation over the spectral range

<sup>a</sup>Full-Width-at-Half-Maximum (FWHM) of response function

range also offered the potential for discovery of hypothesized as well as unexpected lunar surface materials.

[9] The radiometric range was set between 0 and the maximum expected radiance with a 90% radiometric calibration accuracy traceable to a NIST (National Institute of Standards and Technology) standard. The precision performance was specified as a signal-to-noise-ratio (SNR) of >400 for the equatorial reference radiance and >100 for the polar reference radiance. The equatorial and polar reference radiances were designated as the radiance from the Apollo 16 soil reflectance measurement (LR-CMP-117: 67481,70) modeled with 1 AU illumination and solar zeniths of 0° and 80° respectively. The solar irradiance spectrum used for the M<sup>3</sup> baseline characteristics, radiometric modeling as well as measurement analyses is the newKUR spectrum of MODTRAN4 [Berk et al., 1999; Kurucz, 1995]. Other irradiance spectra exist [Thuillier et al., 2004] and may be used to analyze M3 radiance measurements or covert M3 derived products as required. Based on analysis of returned samples, telescopic observations and observations by other instruments over portions of the spectral range, which give an indication of the maximum radiance levels to which M<sup>3</sup> must be sensitive, the saturation radiance was set at 2 X the equatorial reference radiance. Saturation radiance is the radiance level above which the M<sup>3</sup> detector will be "saturated" and not return meaningful estimates of the incident radiation intensity. These reference radiances were established to bracket illumination conditions for a wide range of the planned M<sup>3</sup> measurement scenarios and are shown with the saturation radiance in Figure 3. These radiances were also used to assess and verify the expected performance of spectroscopic algorithms planned for use with the returned M<sup>3</sup> spectra to address the mission goals and objectives.

[10] To pursue the science objectives within the context of Chandrayaan-1 guest instrument constraints, a nominal

spatial sampling of 70 m was specified to capture a wide range and diversity of exposed rock outcrops associated with steep terrain and crater walls as well as to allow measurement of small young craters. A cross-track field of view of 24° (40 km from 100 km altitude) was specified for the pushbroom imaging spectrometer to assure orbit-to-orbit overlap in the presence of spacecraft altitude variation between 80 and 120 km at the 32 km orbit spacing. Both the swath and spatial sampling distance vary as a function of orbital altitude and lunar topography.

[11] For imaging spectrometers using advanced area array detector technology, the specification of spectroscopic measurement uniformity is critical. For M<sup>3</sup>, both the cross-track spectral uniformity and spectral instantaneous-field-of-view (IFOV) uniformity were strictly specified. Figure 4 provides a depiction of the imaging spectrometer uniformity constraints with respect to the measured sample on the surface, the wavelength of light, and the area array detector that captures the spectra. The cross-track spectral uniformity limits the variation in spectral calibration within the full FOV. The M<sup>3</sup> cross-track uniformity was specified at >90%. This requires the spectral calibration to remain within 10% of the 10 nm spectral sample (1 nm) across the full cross-track swath of the imaging spectrometer. Studies of lunar materials have shown that with this level of cross-track spectral uniformity, all spectra from a M<sup>3</sup> spectral image data set may be analyzed in concert. A second critical science measurement characteristic is the spectral IFOV uniformity. The spectral IFOV uniformity requirement limits the variation of the ground sample location as a function of wavelength. For M<sup>3</sup> the spectral IFOV uniformity was set at >90%, ensuring that the IFOV remains centered on the same surface sample at the 90% level from 430 nm to 3000 nm. Failure to constrain IFOV uniformity allows the sample location on the surface to vary with wavelength and violates a fundamental assumption of spectroscopy, namely that at every wavelength the measured value is of the same area of surface sampled. The >90% spectral cross-track and >90% spectral IFOV uniformity requirement for M<sup>3</sup> set a new

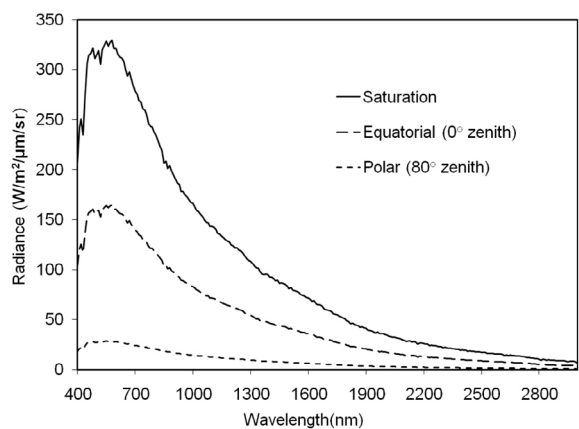


**Figure 3.** Saturation, equatorial and polar reference radiances established for the M<sup>3</sup> imaging spectrometer. The equatorial and polar reference radiances provide the benchmark levels for the SNR performance characteristics.

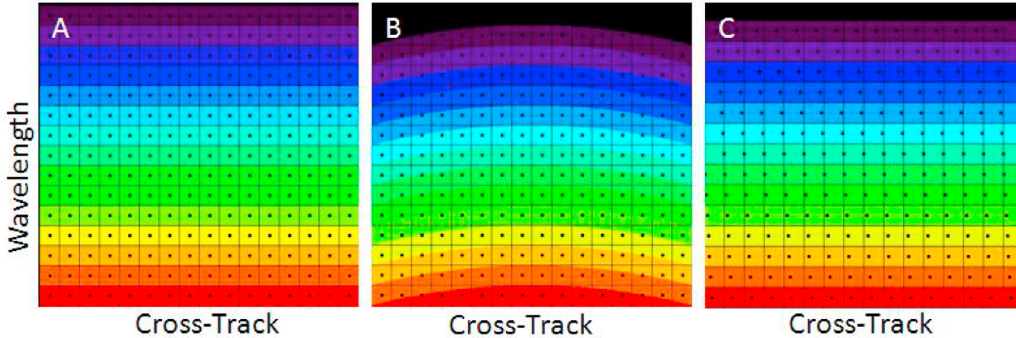


**Figure 4.** Depiction of the pushbroom-type imaging spectrometer uniformity requirement. The dots represent the sample location on the surface. The squares represent the detector array elements. The cross-track color bands correspond to different wavelengths of light. (a) A uniform imaging spectrometer: all cross-track elements have the same spectral calibration and all wavelengths in a spectrum are measured for the same sample. (b) An imaging spectrometer with poor cross-track spectral uniformity: the spectral calibration changes up to 100% in the cross-track direction. (c) An imaging spectrometer with poor IFOV uniformity: the location of the surface sample changes with wavelength, violating a key assumption of spectroscopy.

precedent for measurement quality in space pushbroom imaging spectrometers.

### 3. Imaging Spectrometer Design

[12] The M<sup>3</sup> science measurement characteristics that flowed from the science goals and objectives provided the primary input for selection of the M<sup>3</sup> imaging spectrometer design. However, additional design constraints were derived from a refined understanding of the guest instrument opportunity on board the Chandrayaan-1 mission. Key among these additional constraints were low mass (<10 Kg), limited power, compact volume as well as a constrained data downlink capacity. Beginning with the full set of science measurement characteristics and mission constraints, a complete design including on-orbit and ground elements was developed for the M<sup>3</sup> imaging spectrometer science instrument to enable successful participation in the Chandrayaan-1 mission.

[13] To achieve the science measurement requirements within these constraints, the M<sup>3</sup> instrument design required inclusion of a suite of key enabling elements. First among these was a high uniformity and high throughput imaging spectrometer optical design that is both compact and comparatively simple for development in a limited time period. In order to measure the full spectral range from 430 to 3000 nm with a single spectrometer, an all-reflective Offner design was selected [Mouroulis *et al.*, 2000]. The optical design principles of M<sup>3</sup> have been given by Mouroulis *et al.* [2007]. Figure 5 shows a cross-section of the complete M<sup>3</sup> Offner imaging spectrometer with telescope. In this design, light from the Moon passes through a pair of baffles and is reflected from a fold mirror to a compact three mirror anastigmat telescope. The telescope subsystem provides the 24°FOV in the cross-track direction and the 0.7 milliradian IFOV in the along-track, thus supporting the required 40 km swath and 70 m spatial sampling from the nominal 100 km orbit. Light from the telescope is imaged on a 27 micron wide uniform open slit. Light selected by the slit is passed to

the surface of the spectrometer mirror where it is reflected to the efficiency-tuned diffraction grating. Light is spectrally dispersed with optimized efficiency in the -1 order over the spectral range from 430 to 3000 nm. The spectrally dispersed light from the diffraction grating is reflected for the second time by the spectrometer mirror and selectively transmitted by the order sorting filter and focused on the M<sup>3</sup> HgCdTe area array detector. The order sorting filter is a three zone filter with a nominal cut-on at 425 nm and zone

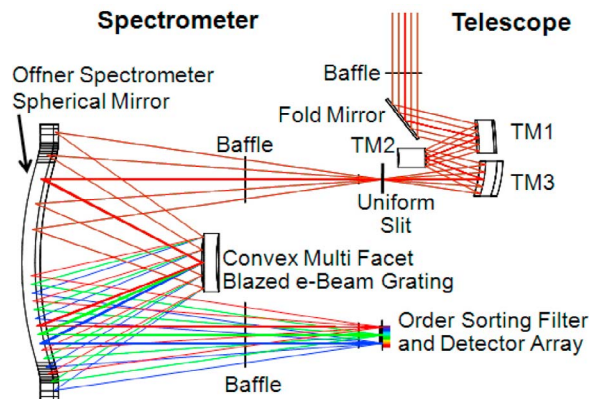


**Figure 5.** Cross section of the compact and simple M<sup>3</sup> imaging spectrometer optical design that provides a high uniformity, full spectrum measurement from 430 to 3000 nm with a 24° cross-track FOV and 0.7 milliradian spatial sampling. Light enters M<sup>3</sup> through a set of baffles (first baffle not shown) to the fold mirror of the small three mirror anastigmat telescope where the light is fed to the uniform spectrometer slit. The light selected by the slit is reflected by the surface of the spectrometer mirror to the efficiency-tuned multifacet-blazed diffraction grating. Spectrally dispersed light from the grating is reflected a second time by the spectrometer mirror, passes through the order sorting filter and is imaged on the full spectral range HgCdTe area array detector for capture by the electronic signal chain.

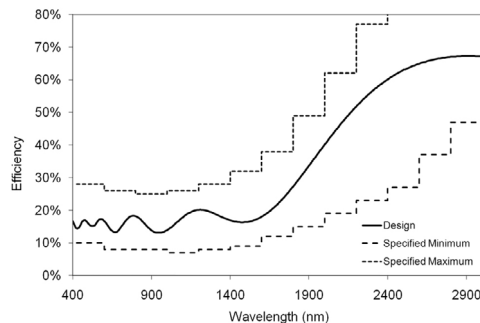


**Figure 6.** Simulated efficiency with requirement limits of the  $M^3$  multifacet blaze diffraction grating. This custom electron beam lithography grating is designed to balance the throughput of the  $M^3$  imaging spectrometer over the broad range from 430 to 3000 nm.

boundaries at 815 nm and 1565 nm. The filter was custom manufactured by Barr Associates Inc. At the detector array the dispersed light is converted to an electronic signal and passed to the electronic signal chain for amplification, digitization, compression, formatting, and storage prior to Chandrayaan-1 transmission to Earth.

[14] A key enabling component for this compact, wide spectral range, and high uniformity imaging spectrometer design is the low-scatter convex grating that is fabricated using electron beam lithography [Maker *et al.*, 2002; Wilson *et al.*, 2003]. For  $M^3$ , an efficiency tuned, multifacet-blaze diffraction grating was custom designed to balance the optical efficiency with respect to the incoming solar reflected spectrum over the full 430 to 3000 nm spectral range [Backlund *et al.*, 2004]. Figure 6 shows the simulated efficiency and the specification limits for the convex  $M^3$  diffraction grating. The ability to tune the grating efficiency and balance the typical lunar signal over the broad spectral range enabled optimal use of the detector array full well with a single nominal integration time as well as to simultaneously meet the broad SNR requirement. While electron-beam lithography diffraction gratings have previously flown in space instruments,  $M^3$  is the first to use a multifacet-blaze convex grating of this type.

[15] Another critical component of the  $M^3$  science imaging spectrometer design is the extended spectral range detector array. Extension of the spectral range this type of detector was first established with the Compact Airborne Spectral Sensor (COMPASS) imaging spectrometer [Simi *et al.*, 2001]. Using a single detector array to span the range from 430 to 3000 nm eliminates the need for multiple detector arrays and signal chains and the corresponding complexity of multiple spectrometers and/or beam splitters that increase design, development, alignment, schedule, and cost factors. The  $M^3$  detector array readout integrated circuit (ROIC) is the TCM6604A device manufactured by Teledyne Inc. For  $M^3$ , this ROIC is used with HgCdTe detector material that has had the substrate removed to allow sensitivity down to 430 nm. The array has 640 by 480 detector elements with 27 micron pitch, a nominal full well of 650,000 electrons, and a read noise of  $\sim$ 100 electrons. The TCM6604A uses a snap-shot readout with integrate-

while-read to preserve uniformity and light collection efficiency. In detail, the device is configured with four 160 by 480 element panels that are read simultaneously providing the full 640 by 480 dimension. To meet the  $M^3$  measurement requirement 600 of the available 640 elements are used for imaging in the cross-track direction to cover the  $24^\circ$ FOV with 0.7 milliradian sampling. In the spectral direction, 260, including margin, of the available 480 elements are used to cover the spectral range from 430 to 3000 nm at 10 nm. The TCM6604A has flown in space on CRISM, however  $M^3$  is the first use in space of a HgCdTe substrate-removed detector with the spectral range extended to visible wavelengths. The extended spectral range is enabling for the  $M^3$  imaging spectrometer design.

[16] With the optical design, grating and detector characteristics established, a comprehensive radiometric model was developed for the  $M^3$  imaging spectrometer. The model includes all of the optical surfaces, the F#, the efficiency of the grating, the detector quantum efficiency and noise properties as well as the digitization characteristics of the electronic signal chain. Thermal control of the detector and spectrometer temperatures are also accounted for in the model. Figure 7 shows the predicted SNR for the  $M^3$  design for the equatorial and polar reference radiances. With this design and specified components,  $M^3$  meets the requirement of an SNR of  $>400$  for the equatorial and  $>100$  for the polar reference radiance.

[17] The optical, thermal, and structural requirements of the  $M^3$  design in conjunction with high level mission requirements led to the selection of diamond-turned 6061 aluminum as the principal material for fabrication of optical, thermal and structural elements. For  $M^3$ , the telescope mirrors and grating have aluminum reflectivity. The spectrometer mirror uses a protected silver coating to increase throughput. To satisfy thermal constraints, the detector array is held in an athermalized titanium mount. Figure 8 shows the design of the opto-mechanical subsystem for  $M^3$ . In order to achieve the uniformity characteristic inherent in the  $M^3$  optical design, the mounts for the grating and detector array include threaded rods that allow fine adjustments and are also lockable to withstand testing, launch and space flight conditions. These fine adjustment mounts are unique and required to allow fine rotation of the grating as well as six degree of freedom adjustment of the detector array in

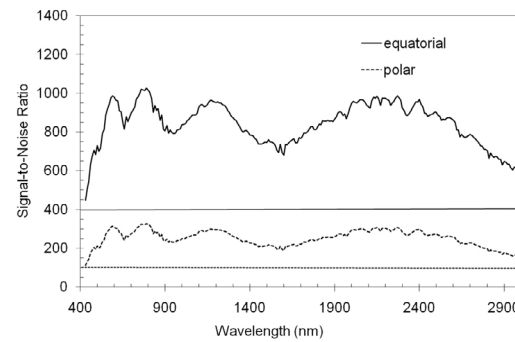


**Figure 7.** The model predicted signal-to-noise ratio for the equatorial and polar reference radiance's based upon the  $M^3$  imaging spectrometer optical, electronics and thermal design.

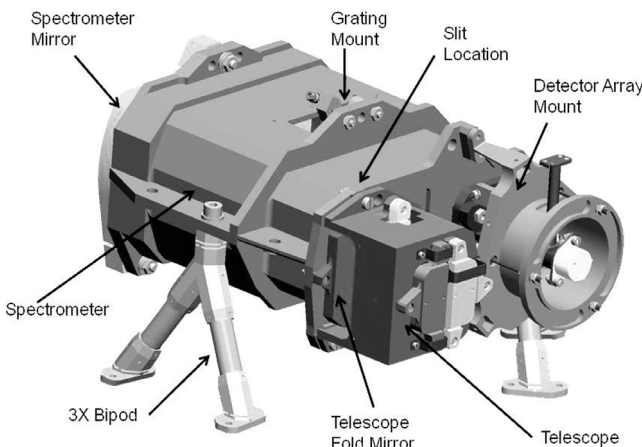


**Figure 8.** Design of the  $M^3$  imaging spectrometer opto-mechanical subsystem. The telescope, spectrometer, slit location, grating mount and detector array mount are shown along with the overall aluminum structure and mounting bipods.

order to achieve  $\geq 90\%$  uniformity requirement with respect to the 27 micron detector array dimension. This uniformity requirement leads to the need for controlled adjustments much finer than 2.7 microns with active feedback in order to position the dispersed spectrum accurately on the detector array. The designed  $M^3$  mounts accomplish controlled adjustments finer than 0.5 microns. This is a driving requirement implemented in the opto-mechanical subsystem design.

[18] In order to provide feedback on dark signal levels and possible scattered light, two key features were included in the spectrometer design. First, the spectrometer slit length was undersized to nominally illuminate only the center 600 cross-track elements of the 640 available detector array elements. Light recorded by cross-track detector elements 11–20 and 621–630, which are outside the central 600 detector element range of the slit and thus masked from direct lunar illumination, provide an estimate of internal scattered light. The second feedback element of the design was to undersize the order sorting filter mask so that cross-track detector elements 1–10 and 631–640 are covered. The signals recorded by these detector elements are available to assess and monitor the nominal dark signal levels of the detector array during image acquisition. Related signal monitoring approaches have been used in the CRISM and MaRS imaging spectrometers.

[19] To achieve the  $M^3$  science measurements in lunar orbit a comprehensive thermal design was required. For noise performance, the HgCdTe detector array with a 3000 nm cutoff wavelength requires cooling to  $< 160$  K with a nominal set point of 156 K. The detector response is not sensitive to temperature change at these nominal temperature levels. In addition, the spectrometer is required to be cooled below 190 K to minimize the contribution of spectrometer-related background photon noise. These cryogenic temperature constraints are exceptionally challenging in the low (100 km) orbit above the Moon where the lunar surface radiating to space reaches temperatures of 400 K under direct illumination. In the design phase both

active and passive cooling options were considered. In order to minimize weight and power and to offer reliability for an extended mission, a first-of-its-kind three stage passive cooler with parabolic reflective elements was adopted [Rodriguez et al., 2009]. This new lightweight and compact design with interleaved flat radiative and parabolic reflective surfaces offered high efficiency radiative cooling for the detector, the spectrometer, and the thermal shield. A depiction of this innovative passive cooler design is shown in Figure 9. A key advantage of this cooler design is the absence of a need for a large deployable Moon shade. To complete the  $M^3$  thermal design multilayer insulation blankets, thermal straps, and optimized surface coatings were used to manage the distribution and transfer of thermal energy.

[20] A complete electronic and computer signal chain was designed to operate the TCM6604A detector array and to digitize, compress, format and store the measurements prior to downlink. In this subsystem the analog signals from the detector array were amplified and then digitized at 12 bit sampling. The frame rate for the detector was specified at 80 hz to allow two reads of the detector during the nominal along-track sampling. The two reads from the detector are immediately summed and effectively double the saturation level during the nominal sampling interval. Following digitization the measured values are passed to the  $M^3$  on-board processing computer and dedicated solid state recorder (SSR). The computer and SSR were not part of the original  $M^3$  proposal, however following discussion with ISRO the requirement for these elements was established. The  $M^3$  computer and SSR design were based on the communication and navigation computer system developed for the NASA Mars Reconnaissance Orbiter (MRO) and at the time of  $M^3$  had been enhanced for the Mars Science Laboratory (MSL). For  $M^3$  the key feature of this computer was the inclusion of 16 gigabits of memory to be used as a simple SSR in a first in, first out (FIFO) mode. The computer also handles the

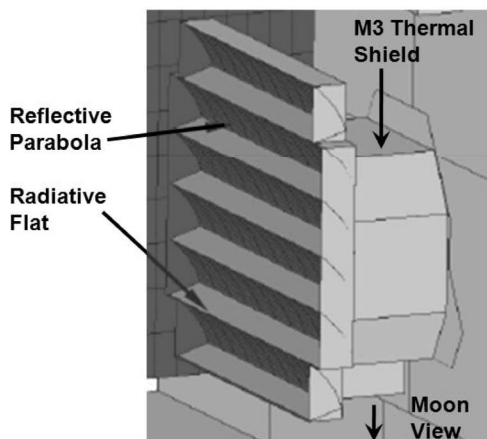


**Figure 9.** Innovative  $M^3$  three stage passive thermal cooler design to control the temperature of the detector array, spectrometer and thermal shield in the 100 km orbit above the Moon. The reflective parabolic surfaces direct the Moon light and thermal radiation away from the radiative surfaces of the passive cooler. Different sets of the flat radiative surfaces cool the detector, spectrometer and thermal shield.

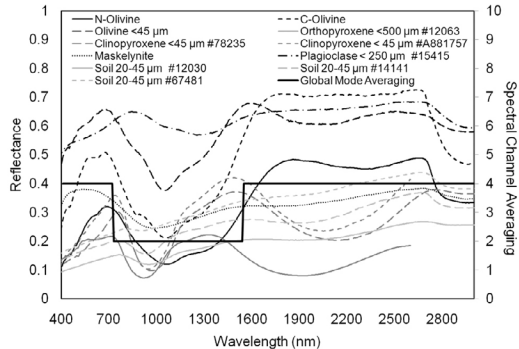


**Figure 10.** Depiction of  $M^3$  averaging of 2 and 4 spectral channels to as part of the proscribed compressing for Global Mode data acquisitions. Higher spectral resolution is maintained in the 700 to 1500 nm region of the spectrum.

instrument temperature, voltage, current, and status telemetry as well as the various states of the  $M^3$  instrument. These instrument states include engineering, survival, decontamination, playback, imaging, and off. The  $M^3$  computer provides the interface between the  $M^3$  instrument and Chandrayaan-1 spacecraft. The measured imaging spectrometer data sets are stored in the SSR and then passed to the spacecraft in Consultative Committee for Space Data Systems (CCSDS) format for transmission to Earth receiving stations upon command.

[21] To meet the lunar science mapping objectives and to accommodate the constraints of the data downlink from the spacecraft to the Earth receiving station, two  $M^3$  instrument measurement modes were designed. The full spectral and spatial resolution measurement mode was designated “Target Mode.” In this mode data are collected at full resolution with 640 cross-track detector elements (600 are lunar surface imaging) and 260 spectral detector elements for every along-track sample with a nominal spatial sampling of 70 m. With a spacecraft velocity of 1544 m/s and 12 bit sampling, this corresponds to a data rate of 44 megabits per second. During the nominal 120 min orbit with half illuminated, the potential per orbit data rate for  $M^3$  is 158 gigabits. An important mission constraint was the 8.3 megabit per second spacecraft downlink rate shared between several high data rate instruments. To allow efficient global reconnaissance with  $M^3$ , a “Global Mode” was developed to collect rapid full lunar coverage at reduced spatial and spectral sampling. The Global Mode of  $M^3$  spatially averages 2X2 spatial elements and designated portions of the spectral range by 2X and 4X. The ranges of spectral averaging are spectral detector elements 1–32 by (4X), 33–116 (2X), and 117–260 (4X). The nominal corresponding wavelengths are 430 nm to 720 nm at 4X, 730 nm 1540 nm at 2X, and 1550 nm to 3000 nm at 4X. This results in a Global Mode data set with 86 spectral channels. The effective compression of Global Mode with respect to Target Mode is 12X. Figure 10 provides a depiction of Global Mode spectral averaging in the context of lunar mineral and soil spectra. To further optimize acquisition of  $M^3$  data, a lossless compression algorithm of 1.5X was added to the electronics design for both Target and Global Mode data. With collection of data over half an

orbit, the baseline data rate with Global Mode and lossless compression the data volume is 8.8 gigabits per orbit that is well within the 16 gigabit capacity of the  $M^3$  SSR. With these measurement modes, a mission mapping strategy was developed to measure the full surface of the Moon in the first 6 Months with Global Mode and acquire as much as 25% of the Moon surface in the final 18 Months of the nominal 2 year mission [Boardman *et al.*, 2011].

[22] In conjunction with the design of the  $M^3$  imaging spectrometer instrument, the  $M^3$  Instrument Ground Data Subsystem (IGDS) was designed to receive all of the  $M^3$  telemetry and downlinked CCSDS packetized data and process them to Level 0, and Level 1b. Level 0 data are reconstructed viewable raw images from the downlinked packets. Level 1b are radiometrically calibrated measurements with associated spectral and spatial calibration files including latitude, longitude and elevation for every sample in the image. The IGDS delivers the  $M^3$  measurement to the science team for validation and processing to higher levels, and is responsible for delivery of the calibrated, Level 0, and Level 1b data to the NASA Planetary Data System (PDS). The  $M^3$  IGDS was designed based upon the data subsystem of the AVIRIS imaging spectrometer [Green *et al.*, 1998] that has been developed and continuously evolved for processing high volumes of imaging spectrometer measurements. A key feature of the IGDS is simple sequential processing with retention of intermediate processing products for rapid analysis and refinement of processing algorithms. This approach is enabled by the availability of reliable low cost disk storage and high speed computers. The full  $M^3$  IGDS computer hardware system with redundancy was designed to fit within a single rack with attached monitor. The data backup approach is through geographically distributed storage of the packetized and level 0  $M^3$  data and processing software and delivery of the full data set to the Planetary Data System (PDS).

[23] The design of  $M^3$  was carefully optimized to balance the full set of science measurement requirements against the constraints of the observational and mission conditions in order to fully achieve the  $M^3$  science goals and objectives. The result of the  $M^3$  design is a high uniformity and high SNR Offner imaging spectrometer that measures the full spectral range from 430 to 3000 nm with a single spectrometer which is light weight (<10 Kg), low power (<20 W) and compact (<50 × 50 × 50 cm). The configuration of the  $M^3$  design with opto-mechanical and electronics subsystems shown is in Figure 11. Key elements of the instrument are the uniform Offner spectrometer optical design, the efficiency-tuned multifacet electron beam lithography diffraction grating, the extended range HgCdTe detector array, the submicron-adjustable mounts lockable for space flight, and the three stage passive cooler with parabolic reflectors.

#### 4. Development, Alignment, and Testing

[24]  $M^3$  was selected as a NASA Discovery Mission of Opportunity in February 2005. The principal design refinement and development efforts began in May 2005 when sufficient resources became available. The Science Requirements Review (SRR) was held on the 26th of June 2005 based on the requirements as specified in the proposal

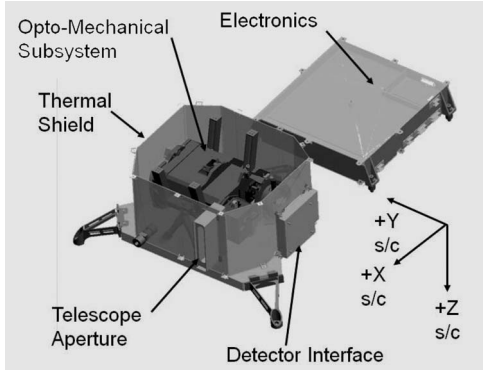


**Figure 11.** Design configuration of the  $M^3$  imaging spectrometer with opto-mechanical, thermal shield and electronics. The passive cooler mounts on top of the opto-mechanical subsystem with thermal links connected to the detector, spectrometer and thermal shield.

in conjunction with improved understanding of the characteristics of the Chandrayaan-1 mission. The Preliminary Design Review (PDR) was held on the 31st of August 2005 and early procurements for key components such as the detector array and order sorting filter were initiated. The Critical Design Review (CDR) was held on the 15th of May 2006. Following the CDR, fabrication and assembly of subsystems proceeded through 2006 and early 2007. In this time frame the spectrometer mirrors, housing, slit, mounts and grating were fabricated. Figure 12 shows a picture of the electron-beam lithography grating, an atomic force micrograph of the multifacet blaze as well as the measured efficiency of the diffraction grating with respect to the specification limits. The telescope mirrors and housing were fabricated and assembled. The detector array and order sorting filter were procured and assembled with the six degree-of-freedom detector mount. The alignment detector signal-chain electronics were developed and tested. The spectrometer and telescope were warm aligned and assembled to form the core of the opto-mechanical subsystem. Figure 13 shows the all-aluminum opto-mechanical subsystem following initial assembly and Figure 14 shows the opto-mechanical subsystem installed in the thermal shield in preparation for alignment and testing.

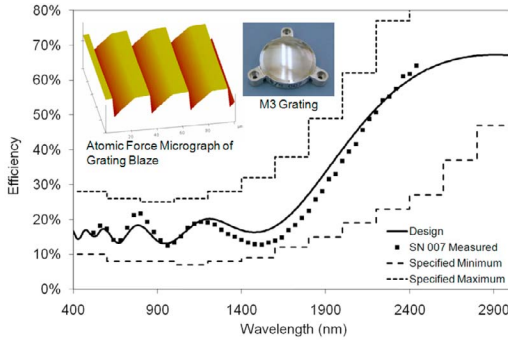


**Figure 12.** The fabricated efficiency tuned  $M^3$  diffraction grating with the measured efficiency as well as an atomic force micrograph of the actual blaze for verification.

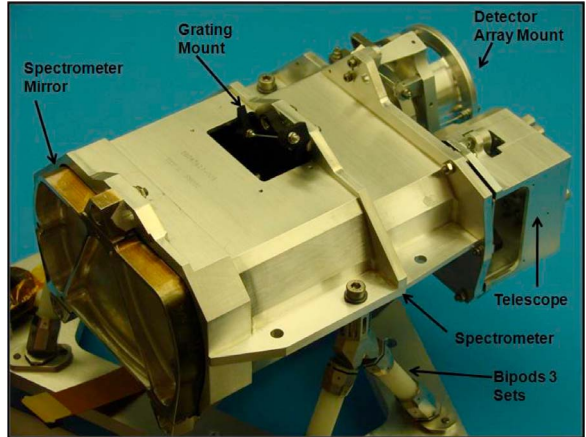


**Figure 13.**  $M^3$  opto-mechanical subsystem in development in 2006 with all key design elements.

[25] In the instrument development period, the light weight and compact  $M^3$  passive cooler was fabricated and tested with special focus on the characteristics and orientation of the enabling parabolic optical reflectors and flat radiative surface. Figure 15 shows the  $M^3$  passive radiator cooler during development with interleaved radiative and parabolic reflective panels. This cooler enables operation of the cryogenic detector in a 100 km lunar orbit with surface temperatures varying between 400 K and 70°K.

[26] In parallel with the development of the opto-mechanical and thermal subsystems, the detector interface electronics and  $M^3$  computer with SSR were fabricated and tested. For the IGDS the computer hardware was procured and software processing tools were procured and developed. The existing set of imaging spectrometer test, alignment, and calibration analysis tools were updated and adapted to support the alignment and calibration phase of  $M^3$  development.

[27] Following integration of the opto-mechanical subsystem and laboratory test electronics, early testing of  $M^3$  was performed in a thermal vacuum chamber beginning in late 2006. For testing, alignment and calibration of  $M^3$ , optical sources were viewed through a 10 cm diameter sapphire window in the  $M^3$  thermal vacuum chamber. The

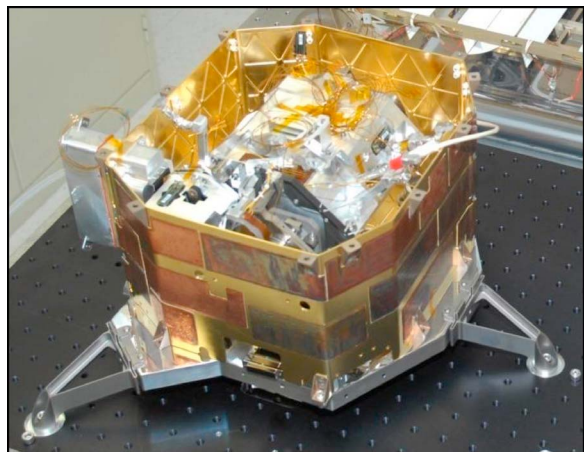


**Figure 14.** Opto-mechanical system including telescope, spectrometer and detector array installed in  $M^3$  thermal shield in preparation for testing and alignment.



**Figure 15.**  $M^3$  passive cooler in test during instrument development. This compact passive cooler with interleaved reflective and radiative elements is the first of its kind for spaceflight and is enabling for the  $M^3$  imaging spectrometer.

transmittance of the sapphire window was measured independently with a Cary 5000 laboratory spectrometer over the full spectral range and is shown in Figure 16. The vacuum chamber window is nearly spectrally uniform over the full  $M^3$  spectral range to 3000 nm. Early cold testing was used to verify the basic functionality of the  $M^3$  imaging spectrometer with a full imaging spectrometer measurement suite acquired on the 15th of December 2006. The measurements included a dark signal measurement with the vacuum chamber shutter closed, an illuminated Spectralon (Labsphere, Inc) panel measurement, and a measurement from a custom neodymium oxide panel with distinct spectral features. The dark signal levels were subtracted and a ratio formed between the neodymium oxide and Spectralon panels. This ratio was the first reflectance spectrum measured by the  $M^3$  imaging spectrometer and is shown in Figure 17. The spectrum is presented in comparison to a spectrum measured over the range 400 to 2500 nm by an ASD full range point spectrometer (ASD Inc.). The ASD

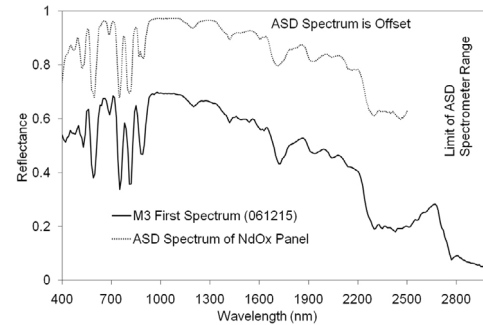


**Figure 17.** First spectrum measured by the  $M^3$  imaging spectrometer in the laboratory on the 15th of December 2006. The strong absorption features of the neodymium oxide panel are measured across the spectral region. The ASD spectral range is limited to 2500 nm.

reports data with 1 nm sampling. The ASD spectral response function FWHM is  $\sim 3$  nm in the 350 to 1000 nm range and  $\sim 8$  nm in the 1000 to 2500 nm range. This first spectroscopic light measurement verified that the  $M^3$  design and development of the opto-mechanical, thermal and electronics subsystems were on track to meet the science measurement requirements.

[28] Six cold cycles in the thermal vacuum chamber were used to align and test  $M^3$  in preparation for calibration. Cold cycle measurements from  $M^3$  were typically initiated with a chamber shutter closed dark signal measurement followed by measurements of the spectral, radiometric and spatial illumination sources. To measure the full 24°FOV of  $M^3$  through the restricted 10 cm thermal-vacuum chamber window,  $M^3$  was mounted on a rotation stage. Figure 18 shows the dark signal image as well as an illuminated image from a radiometric test source with use of the rotation stage. These images are from spectral channel 64 (1034.9 nm). The dark signal image has vertical stripes due to fabrication differences in the individual detector element offset characteristics. The radiometric source image shows a high signal diagonal band formed as  $M^3$  is rotated to view the source. In this illuminated image, the vertical stripes are due to both detector element gain and offset variation. From these measurements the total, dark and total minus dark signal levels in all spectral channels may be calculated as shown in Figure 19 for cross-track sample 300. The signal peaks at the long wavelength channels because  $M^3$  performance is optimized for the infrared and the laboratory radiometric source is less intense at short wavelengths. At spectral channels 41 and 116 the seams of the order sorting filter cause reduced signal spikes. A detector element with high offset is present at channel 182 for this cross-track sample. Figure 20 shows the average dark signal for the full dark signal image with 640 cross-track and 260 spectral detector elements. The boundaries between the four detector panels at 161, 321 and 481 are apparent as are single detector elements throughout the image with anomalously high dark signal levels. Other variations in the dark signal image are due to detector material variation and variation in the underlying 6604a readout integrated circuit. Figure 21 shows the standard deviation of this test dark signal image. In this image, anomalous detectors elements with

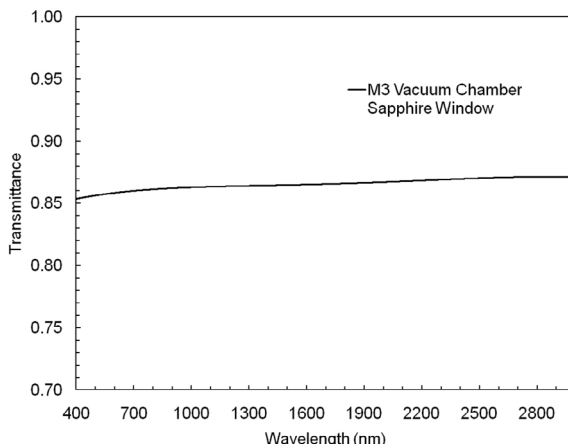


**Figure 16.** Measured transmittance of the sapphire window in the thermal vacuum chamber used for cold testing, alignment and calibration of the  $M^3$  imaging spectrometer.

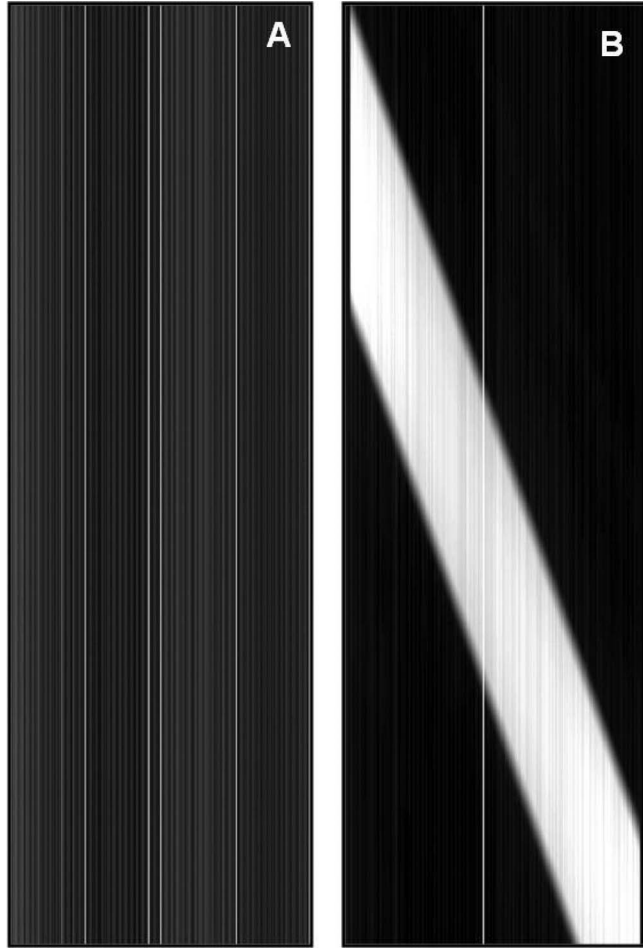


**Figure 18.** (a) Dark signal measurements from M<sup>3</sup> spectral channel 64 showing detector to detector variability. (b) Measurement from illuminated radiometric source with M<sup>3</sup> rotated in the thermal vacuum chamber to capture the 24°FOV.

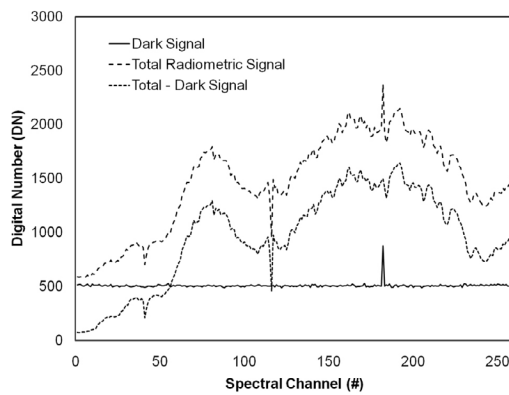


**Figure 19.** Example signal levels from M<sup>3</sup> for cross-track sample 300 measured during radiometric testing. The order sorting filter seams are present at spectral channel 41 and 116 and a detector element with high offset is present at channel 182.

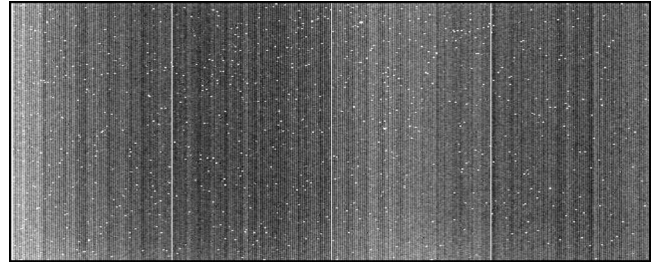


**Figure 20.** Average dark signal image showing typical variation for all 640 detectors in the cross-track direction and 260 detectors in the spectral direction. The bright columns 161, 321, and 481 are the boundaries of the four zones of the M<sup>3</sup> TMC 6604a detector array. Scattered throughout the array are detectors with anomalously high dark signal values.

high variability are identified within the detector array. To create a complete cross-track calibration frame of the radiometric source, the diagonal band of the data set is extracted over the full FOV, producing a 640 cross-track by 260 spectral channel data set. The extracted diagonal of the average M<sup>3</sup> response to the radiometric source with dark signal subtracted is shown in Figure 22 for all cross-track and spectral detector elements. In this Target Mode image the filter seams are evident centered at spectral channels 41 and 116 across the FOV. The detector's output panel zone boundaries are evident, as are the vignetted and masked regions of the edges of the detector array that are used to assess scattered light and dark signal levels. Anomalous non-responsive detector elements appear as single detector low values in the image. A fixed ripple pattern associated with an interference effect between the surface of the detector array and the order sorting filter is present in the lower portion of this average signal image. During radiometric source testing late in development a scattered light effect associated with an unruled annulus of the diffraction grating was identified. Figure 23 shows the estimated fraction of scattered light with respect to wavelength for the laboratory radiometric illumination source. The vignetted left and right sides of the detector array were specifically included in the M<sup>3</sup> design to enable assessment and compensation of scattered light. Subsequent designs of the M<sup>3</sup>-type spectrometer have eliminated this source of scattered light.

[29] The linearity of the M<sup>3</sup> imaging spectrometer detector signal-chain was measured in the laboratory with an

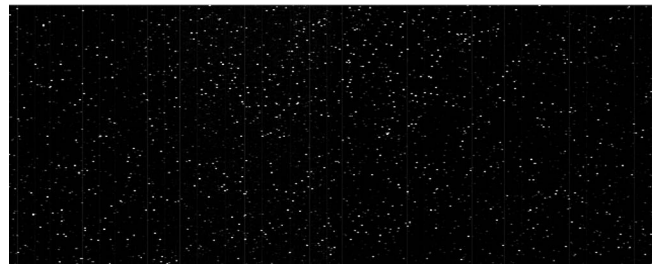


**Figure 21.** Standard deviation of the dark signal test image. A number of detector elements with anomalously high standard deviations are easily identified and mapped.

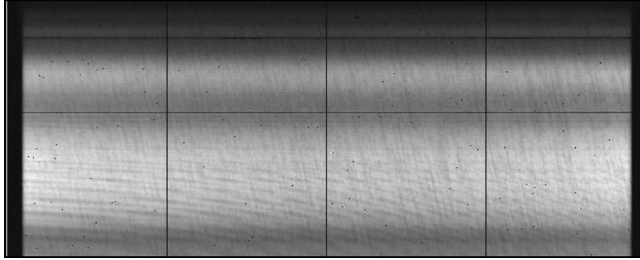


**Figure 22.** Example extracted diagonal image with dark signal subtracted from the radiometric source. The full FOV is captured left to right and full spectral range from short to long wavelength top to bottom. The two horizontal order sorting filter seams are present at spectral channels 41 and 116. The detector array panel zone boundaries are evident a detector columns 161, 321 and 481. The vignetted and masked zones used to assess scattered light and monitor dark signal levels are shown. Anomalous detector elements appear as single point low values in the image. A fixed ripple pattern associated with the order sorting filter is present in the lower (long wavelength) portion of the image.

adjustable integrating sphere (Optronics QL-455). The integrating sphere has a monitoring silicon photodiode which provided luminance values that are recorded at each position of the variable slit used to attenuate the lamp input to the integrating sphere. M<sup>3</sup> was illuminated with series of evenly spaced stepwise intensities from high to low signal levels. A set of 100 detector array measurements were acquired and averaged at each signal level. The average intensity values in each step over the full 12 bit signal range is shown in Figure 24. The M<sup>3</sup> detector signal-chain is shown to be linear over most of the range with a small nonlinearity occurring at the lowest signal levels. The low signal nonlinearity is well characterized with the full set of measurements.

[30] For spectral testing and alignment, M<sup>3</sup> measured a series of spectral sources including a custom laser-fed

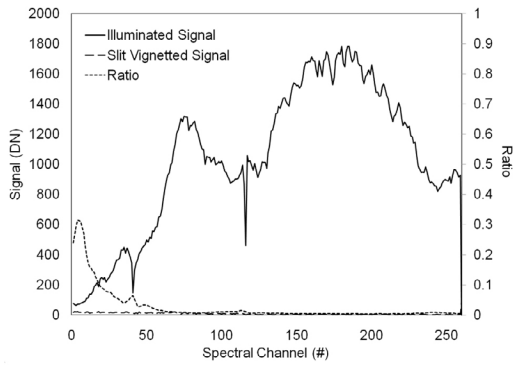


**Figure 23.** Fraction of scattered light as a function of wavelength identified late in M<sup>3</sup> development. This scattered light anomaly is dominate in the shortest wavelengths of the M<sup>3</sup> spectral range. The source of the scattered light has been mitigated in subsequent M<sup>3</sup>-type spectrometers. In M<sup>3</sup> the slit vignetted portion of the detector array enables assessment and compensation for scattered light effects in science calibration processing.

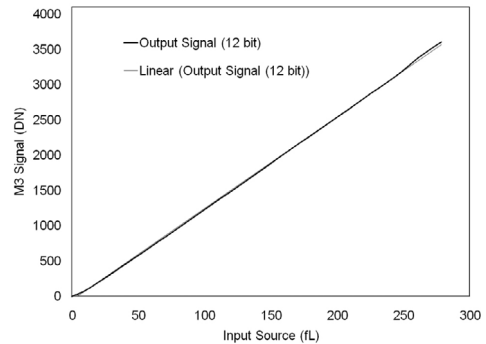


**Figure 24.** M<sup>3</sup> 12 bit detector signal-chain linearity measured during laboratory characterization with a finely adjustable integrating sphere. The M<sup>3</sup> signal chain is linear over most of the range. A small non linearity occurs at low signal levels that characterized with these measurements and compensated in science data calibration processing.

integrating sphere as well as the Neodymium Oxide panel shown in Figure 17. As with the radiometric measurements, these spectral measurements were acquired by rotating M<sup>3</sup> in the vacuum chamber to measure all elements in the full cross-track FOV. Figure 25 shows the extracted diagonal image for the laser sphere viewed by M<sup>3</sup> with dark signal subtracted. Figure 26 shows a spectrum with the signal levels from the 532.3, 1064.5 and 2064 nm lasers.

[31] For M<sup>3</sup> spatial testing and alignment a white light slit illuminating a collimator was used. To assess cross-track focus M<sup>3</sup> was rotated in the vacuum chamber while viewing the white light slit source. Figure 27 shows a portion of the slit image. A set of the cross-track spatial response functions derived from this data set are shown in Figure 28. The normalized cross-track spatial response functions have a full-width-at-half-maximum of 1.1 spatial samples and met the corresponding science measurement requirement.

[32] Analysis of measurements acquired in the development, alignment and testing phase of M<sup>3</sup> showed the occurrence of two anomalous features of the detector array that have also been observed at various levels in the CRISM and MaRS imaging spectrometers that use versions of the TCM6604A detector array. The first is a small negative electronic panel ghost (EPG). When a bright source, such as a laser, illuminates a location in one of the four 160 cross-track element panels of the detector, a small reduction in

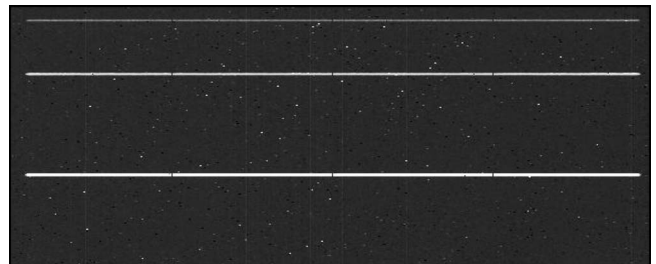


**Figure 25.** Extracted diagonal image from laser sphere source to test and align the M<sup>3</sup> spectrometer. Laser wavelengths of 532.27, 1064.5 and 2064 nm were illuminated. The M<sup>3</sup> spectral range spans 430 to 3000 nm top to bottom.

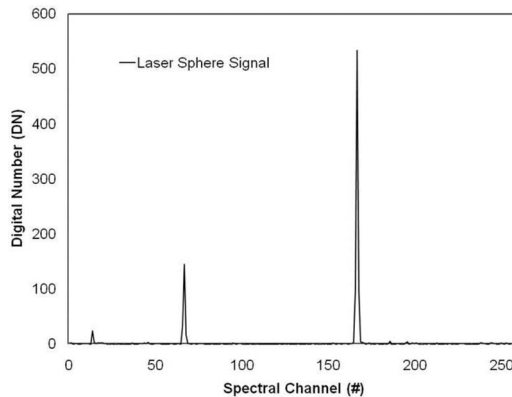


**Figure 26.**  $M^3$  measured signals from the laser sphere during test and alignment.

signal is expressed in the corresponding location of the other three 160 cross-track element panels of the detector array. This electronic panel ghost was assessed as a less than 1% effect. A second feature of the detector array signal chain was identified with the masked columns of the detector array. As the level of illumination was increased the values of the masked detectors for monitoring the dark signal levels of the array dropped by a small proportion. These masked detector elements provide the capability to assess and compensate for this dark pedestal shift (DPS) effect. Throughout the alignment and testing phase of development, the as-built properties of  $M^3$  were characterized and assessed to enable compensation and calibration algorithms such that the science measurement requirements could be achieved on-orbit.

[33] A fundamental science measurement requirement of  $M^3$  is the >90% cross-track spectral uniformity and the >90% spectral IFOV uniformity minimum to maximum across the FOV. These requirements and optical focus were a primary objective of the alignment effort during the laboratory thermal vacuum cycles. During these cycles spectral and spatial uniformity illumination sources were observed by  $M^3$  at operational temperature. These measurements were rapidly analyzed to assess focus and uniformity alignment. In the warm period between each cold

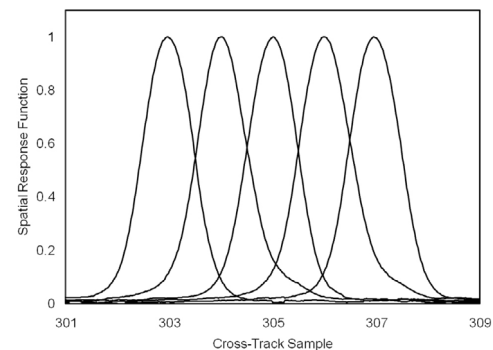


**Figure 28.** Measurement of spatial response function during cold testing and alignment with  $M^3$  viewing a collimated broad band light illuminated slit.

cycle the calculated adjustments were implemented using the custom optical component mounts and feedback mechanisms. Figure 29 shows the cross-track spectral calibration uniformity achieved at the end of cold cycle 6. To assess uniformity, a line is fit to the data to compensate for noise in the measurements. At this point the cross-track uniformity is >95% over the full field-of-view. Figure 30 shows the spectral IFOV uniformity at the end of cold cycle 6 at a level of >95%. With these alignment validation results, the critical science measurement uniformity requirements of  $M^3$  were achieved. Following completion of alignment, the  $M^3$  instrument was prepared for a comprehensive set of calibration measurements and cold cycle 7 in the Month of April 2007.

## 5. Laboratory Characterization and Calibration

[34] Laboratory calibration of  $M^3$  proceeded through collection of measurements from spectral, radiometric and spatial sources that were independently traceable to absolute standards. These measurements were acquired with the detector at the nominal operational temperature of 156 K as well as  $\pm 3$  K from nominal. All measurements were acquired with  $M^3$  viewing the sources through the sapphire window of the thermal vacuum chamber. Dark signal data sets were acquired with a cold shutter prior to each set of

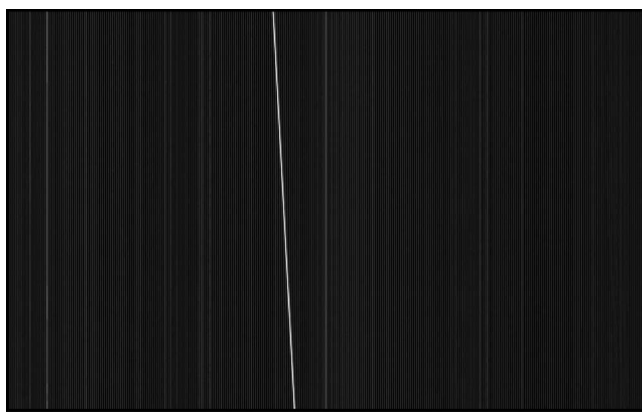


**Figure 27.**  $M^3$  rotation stage image of the collimated broad band illuminated slit for measurement of the cross-track spatial response functions.

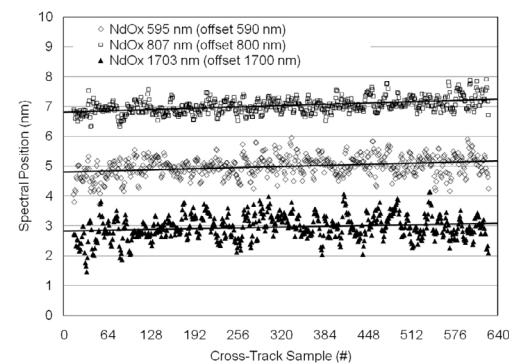


**Figure 29.** Spectral cross-track uniformity calculated from NdOx panel spectral fit of absorption features at 595 nm, 807 nm and 1703 nm. The spectral cross-track uniformity is >95% and exceeds the science measurement requirement.

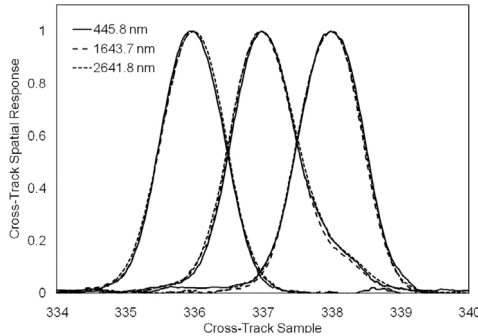


**Figure 30.** Measured spectral cross-track response functions following cold cycle 6 for wavelengths 545.8 nm, 1643.7 nm and 2641 nm. The alignment is >95% over the  $M^3$  spectral range and exceeds the spectral IFOV uniformity science requirement.

calibration source measurements. These calibration measurements from the completed  $M^3$  instrument were acquired in cold cycle 7 and augmented with measurements from cold cycle 6.

[35] The spectral position and response functions were determined with a collimator illuminated by a scanning monochromator (Princeton Instruments Inc, ACTON SpectraPro 500i) with a spectral calibration accuracy of 0.1 nm. The spectral calibration was validated with respect to the 532.27 nm, 1064.53 nm and 2065 nm wavelengths laser integrating sphere. The monochromator wavelengths were correlated to the  $M^3$  measured data by introducing systematic pauses in the scan every 2 nm and long pauses every 200 nm. A spectral channel peak signal method was used to derive the throughput of the  $M^3$  instrument and monochromator collimator system. This method fits a curve to the peak signal for each measured spectral response function. This curve is then used to normalize the throughput at each measured wavelength. Figure 31 shows the normalized  $M^3$  data extracted for a portion of a monochromator scan with synchronization steps. Figure 32 shows a set of extracted spectral response functions for the 1550 nm to 1750 nm portion of the  $M^3$  spectral range. The

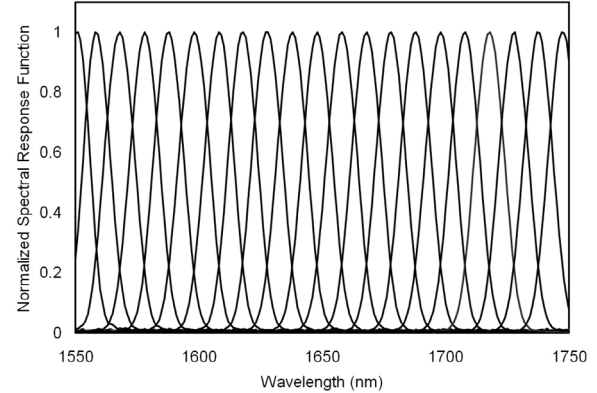


**Figure 32.** Extracted set of normalized spectral response functions over a portion of the spectral range from the scanning monochromator-collimator laboratory calibration of  $M^3$ .

total spectral range of  $M^3$  from spectral channel 1 to 260 in Target Mode was measured and found to span the wavelengths from 406.1 to 2991.2 nm with a sampling interval of 9.981 nm. This spectral range was within the margin of the spectral range requirement of  $430 \pm 50$  nm and  $3000 \pm 50$  nm. The average full-width-at-half-maximum of the spectral response function was determined to be 12.49 nm and was within the requirement range of 10 to 15 nm. The  $M^3$  spectral response functions are well approximated by a Gaussian function as shown in Figure 33 for spectral channel 27. To produce a consistent set of spectral positions and FWHM and to compensate for data dropouts, a third order polynomial was fit to the FWHM variations and a linear function was fit to the spectral channel positions. The resulting nominal spectral channel positions and response function FWHMs for all 260 Target Mode spectral channels are plotted in Figure 34. With determination of the Target Mode spectral positions and spectral response functions, the Global Mode spectral calibration characteristics are determined with convolution-corrected 2 and 4 spectral channel sums.

[36] Radiometric calibration was performed by collection of measurements from a calibration panel illuminated by a

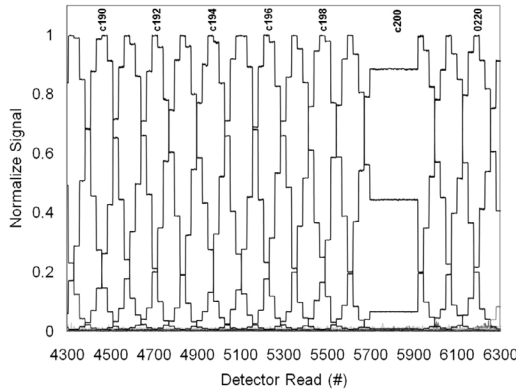


**Figure 31.** Portion of scanning monochromator-collimator data set showing wavelength synchronization steps. The small steps are every 2 nm. The large step indicates 2400 nm wavelength.

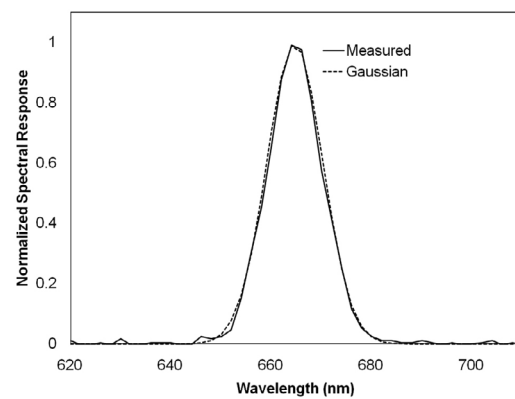


**Figure 33.** Measured spectral response function of channel 27 and corresponding fit of a Gaussian function defined by the spectral position and FWHM.

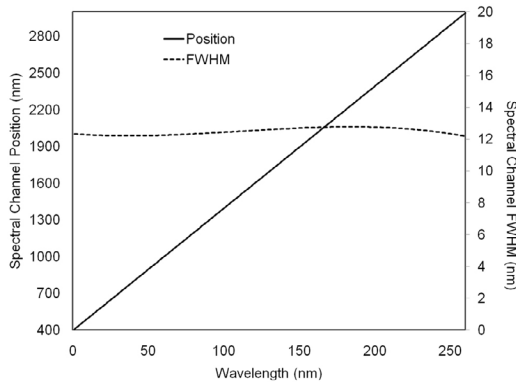


**Figure 34.** The positions and FWHM for the equivalent Gaussian functions that describe the 260  $M^3$  Target Mode spectral channels from 430 to 3000 nm. To populate all channel values from the laboratory measurements the spectral positions are interpolated with a linear function and the FWHM with a best fit third order polynomial function.

NIST traceable 1000 quartz halogen lamp (Labsphere inc. #1131). This lamp was procured with a NIST traced irradiance calibration and uncertainty over the range 400 to 3000 nm. Figure 35 shows the irradiance and uncertainty in the irradiance of the lamp over this spectral range. The lamp was held in a well-baffled calibration fixture  $50 \pm 0.1$  cm from the  $12 \times 12$  inch reflectance calibration panel. Two different reflectance panels (Labsphere Inc.) were used to span the full spectral range from 400 to 3000 nm. A reflectance calibrated Spectralon panel (SN: 50119-1-1) was used from 400 to 1700 nm and an Infragold (SN: 50205-1-1) panel was used from 1700 to 3000 nm. Figure 36 shows the reflectance of the  $M^3$  Spectralon and Infragold calibration panels at the  $0^\circ$  illumination and  $45^\circ$  observation angle geometry used for  $M^3$  radiometric calibration. This split panel approach was adopted to avoid uncertainty and possible artifacts in the radiometric calibration from absorption features in Spectralon above 2000 nm and the absorption features in the Infragold below 1000 nm.  $M^3$  viewed the illuminated calibration panel through the sapphire window in the thermal vacuum chamber. The measured transmittance of the sapphire window is shown in Figure 16. To

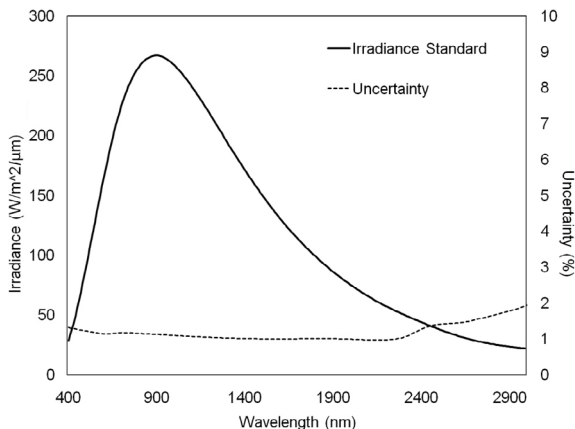


**Figure 35.**  $M^3$  laboratory calibration irradiance lamp standard source with uncertainty.

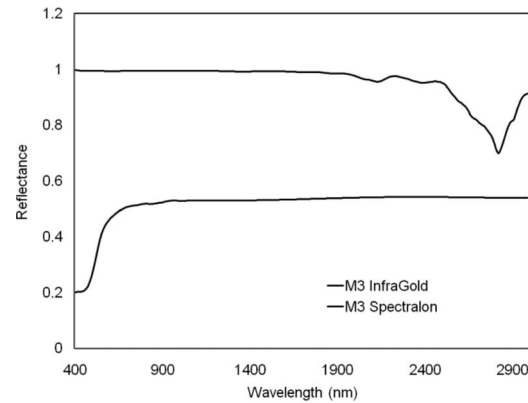


**Figure 36.** Reflectance of  $M^3$  radiometric calibration panels at  $M^3$  laboratory calibration geometry. Spectralon is used in the range from 400 to 1500 nm and Infragold used in the range from 1500 to 3000 nm.

minimize error in radiometric calibration due to atmospheric water vapor absorption over the 1.5 m path length of the calibration apparatus, the radiometric calibration beam path was housed in an enclosure purged with ultra dry air. Humidity and temperature levels were monitored in the enclosure during radiometric calibration measurements. Figure 37 shows a MODTRAN [Berk et al., 1998, 1999] radiative transfer code modeled transmittance for a standard atmosphere and the low humidity atmosphere in the  $M^3$  laboratory radiometric calibration enclosure. The transmittance of a  $1 \mu\text{m}$  path of liquid water and ice are shown as well. The water vapor absorption occurs short of 2800 nm or 2.8 microns. In regard to the  $M^3$  volatile compound science objectives, it is important to note that the water vapor absorption occurs as a doublet shifted to shorter wavelengths than the corresponding absorption feature of liquid water or ice.

[37] For full FOV radiometric calibration, data were acquired viewing the Spectralon panel illuminated by the

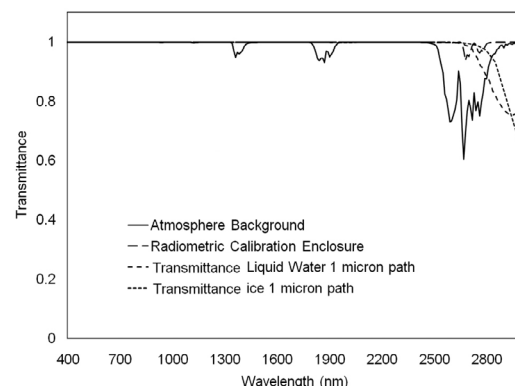


**Figure 37.** Transmittance of a 1.5 m path in the laboratory at background humidity and under ultra dry conditions of the radiometric calibration enclosure. The water vapor absorption is short of 2800 nm or 2.8 microns. For comparison, the modeled transmittance of a 1 micron path through liquid and ice phases of water are shown, exhibiting have absorption features shifted to longer wavelengths.

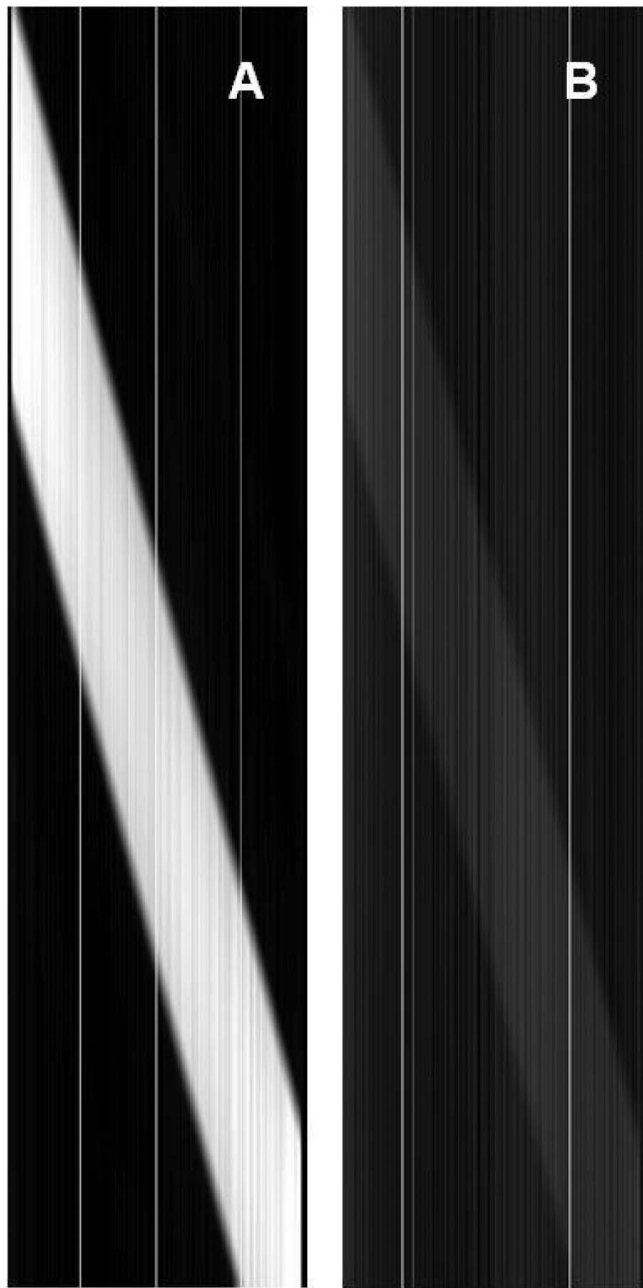


**Figure 38.** (a) Total and (b) background signals measured by  $M^3$  for the Spectralon radiometric calibration source across the full field of view.

NIST-traced lamp while  $M^3$  was rotated on the stage within the vacuum chamber, as described previously. A background measurement was then acquired viewing the panel with a shutter in front of the NIST-traced lamp while  $M^3$  was rotated across the full field of view. Subtraction of the background measurement from the illuminated measurement compensates for indirect illumination sources in the radiometric calibration system. Figure 38 shows an illuminated (A) and background (B) signal image from the Spectralon radiometric calibration source. Figure 39 shows the extracted spectrum for the center 40 cross-track samples along the diagonal for both the total and background illumination conditions as well as the difference signal. An

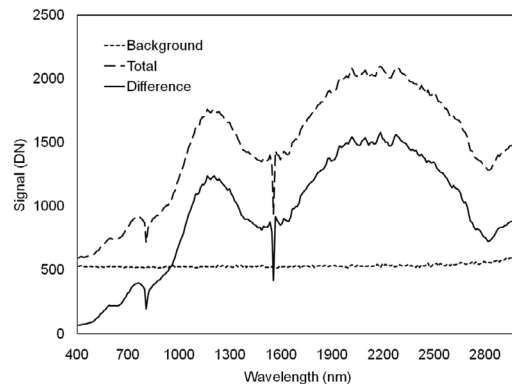


**Figure 39.** The extracted total and background signal for the center 40 cross-track elements along the diagonal. The difference signal is also shown. The background signal rises at wavelengths longer than 2500 nm due to the background emitted radiance from the warm baffles of the calibration apparatus.

equivalent set of measurements were completed for the radiometric calibration source with the Infragold panel. From these measurements, the radiometric calibration coefficients were calculated as the ratio of the NIST traced illuminated radiance from the panel to the  $M^3$  measured background corrected signal. The calibration source radiances were corrected using the transmittance of the thermal-vacuum chamber window and residual atmospheric water vapor absorption. Figure 40 shows the radiometric calibration coefficient values calculated for the Spectralon panel and the Infragold panel merged at 1700 nm with calibration uncertainty. The uncertainty is calculated as the root-sum-squared uncertainties of the lamp irradiance, panel reflectance, panel distance, and vacuum chamber transmittance. In order to relate these radiometric calibration coefficient values to every cross-track element of the  $M^3$  imaging spectrometer, a flat field image was calculated as the ratio of the signal of the center 40 cross-track elements

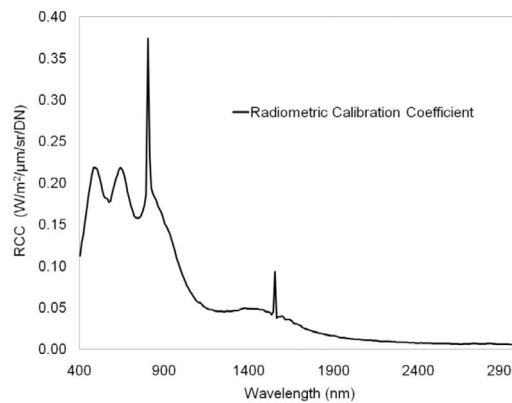


**Figure 40.**  $M^3$  calculated radiometric calibration coefficients with uncertainties. The two spikes are introduced by attenuation of the signal at the order sorting filter seam boundaries. The oscillatory structure in the 500 to 1000 nm region is largely caused by variation in the grating efficiency over this spectral region.

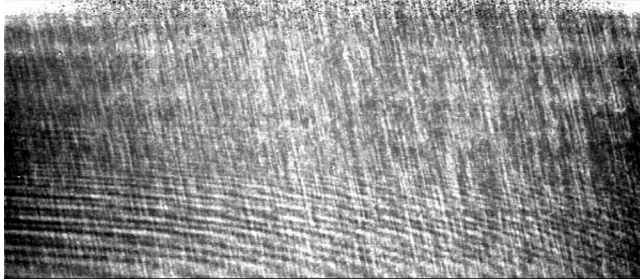


**Figure 41.** Laboratory flat field image for the  $M^3$  imaging spectrometer, calculated from the Spectralon radiometric calibration standard. The ripple toward the longer wavelengths is caused by interference between the order sorting filter and the detector array. The vignetted and masked edges of the detector array are replicated from the last usable cross-track element.

to each cross-track element for all spectral channels. The flat field image for the Spectralon radiometric calibration standard is shown in Figure 41. This laboratory flat field image describes residual throughput variation from a uniform source for the full system in both the spectral and cross-track domains of the detector array. To give an indication of the distribution of the flat field levels, 90% of the values were between 0.902 and 1.096. The structure in the flat field image derives from the optical throughput of the system and the properties of the detector array. Across the flat field image the levels are higher the center and lower toward the left and right edges. This is attributed to a weak optical vignetting effect. The ripple toward the bottom of the flat field (longer wavelengths) is attributed to an etalon-effect between the order sorting filter and the detector array. Other fine scale features including the near vertical structures are associated with the responsivity of the detector array and are a function of the detector material growth and processing. These flat field structures were observed to be stable during laboratory calibration and thermal testing.

[38] The as-built SNR characteristics of the  $M^3$  instrument were calculated using the radiometric calibration measurements and the radiometric model for the equatorial and polar reference radiances. The radiometric model was updated to the as-built system by comparison of the model predicted

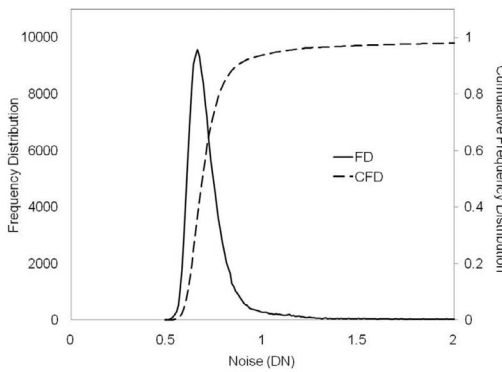


**Figure 42.** Laboratory measured noise properties of the  $M^3$  imaging spectrometer. The median value is 0.66 DN and 90% of the values fall below 0.86 DN.

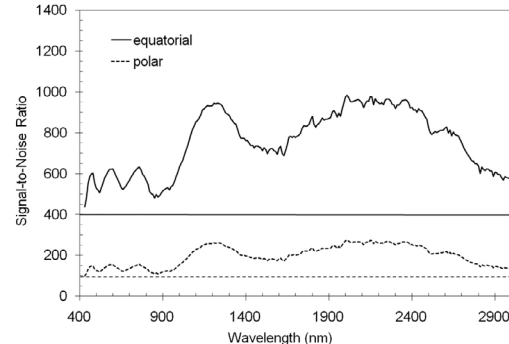


**Figure 43.**  $M^3$  laboratory calculated SNR with radiometric model updated from laboratory measured throughput and laboratory measured noise properties.  $M^3$  meets both the equatorial and polar SNR requirements.

response for the Spectralon radiometric calibration source to the actual instrument measured response from the radiometric calibration sources. In addition, the radiometric model was updated with the measured noise performance at the operational temperature in the thermal vacuum chamber. Figure 42 shows the frequency distribution and cumulative frequency distribution for  $M^3$  noise determined in the laboratory for the nominal operational temperature of 156 K. The measured median noise performance is 0.66 DN and 90% of the values fall under 0.86 DN. The electron to DN conversion factor is 202 electrons/DN. Figure 43 shows the as-built SNR performance calculated from the updated radiometric model for the  $M^3$  equatorial and polar reference radiances.  $M^3$  exceeds the required SNR of 400 and 100 for the respective equatorial and polar reference radiances.

[39] The spatial characteristics of  $M^3$  were measured during the laboratory calibration phase in a manner similar to the alignment phase. Key spatial IFOV characteristics were measured with a collimator fed by a 100 micron illuminated slit. As in the alignment phase,  $M^3$  was scanned in the cross-track direction with respect to the slit to determine the cross-track spatial response function. With these calibration measurements, the cross-track IFOV was found to

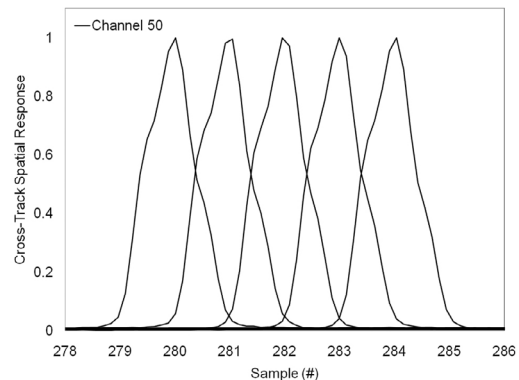


**Figure 44.** Cross-track spatial response functions measured during calibration in Global mode. An asymmetry is present that is induced by finalization of the detector array flight electronics. The FWHM of the response functions meets the requirements.

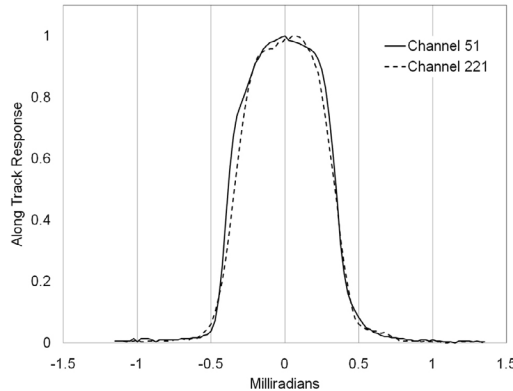


**Figure 45.** Along-track response function of  $M^3$  measured with a collimated illuminated slit translated parallel to the  $M^3$  imaging spectrometer slit.

have an unexpected asymmetry. The cause was isolated to the final configuration of the detector array flight electronics. Figure 44 shows the measured cross-track IFOV for  $M^3$  in Global Mode. The asymmetry was shown to be uniform and within the  $M^3$  cross-track IFOV response requirement. The static along track response function was measured by scanning the slit in the collimator in the along-track direction. The static along-track response function is shown in Figure 45. The on-orbit along-track measurement response function may be calculated by convolution of the static along-track response function with the  $M^3$  orbital integration interval. An additional key spatial calibration characteristic of  $M^3$  is the along-track position for each spatial sample over the cross-track FOV. During the optical design optimization process, in order to achieve high cross-track spectral uniformity and spectral IFOV uniformity, the projection of the  $M^3$  slit on the surface was allowed to have a curved function. The instrument slit is straight, but the projected slit image on the surface through the compact multimirror aspheric surface telescope is curved. Once characterized and included in the  $M^3$  camera model the curved slit function is fully compensated in the orthographic projection of the measurements on the curved and topographically rugged surface of the Moon. This  $M^3$  cross-

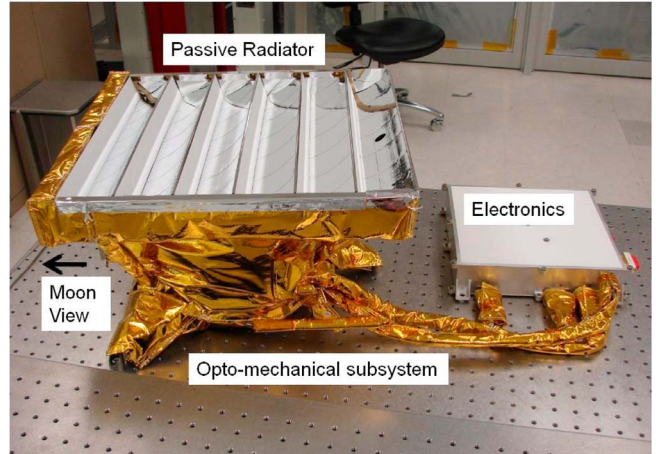


**Figure 47.** Completed  $M^3$  imaging spectrometer with optical bench, passive cooler radiator, cables and electronic box prior to shipment to India.

track projected slit function was measured during laboratory calibration. Figure 46 shows both the designed and measured the cross-track slit function over the 24°FOV of the instrument. This measured function is used to develop the camera model that is in turn used to project the measured spectra to the surface of the Moon [Boardman et al., 2011].

[40] The cross-track spectral calibration uniformity and spectral IFOV uniformity were verified in the laboratory calibration and found to be in agreement with the final alignment uniformity characteristic shown in Figures 28 and 29. The laboratory calibration of  $M^3$  was completed at the end of April 2007 immediately prior to the instrument pre-ship review. All  $M^3$  calibration measurements were stored at distributed locations and a complete set was delivered to the Planetary Data System (PDS) for long-term archive.

## 6. Instrument Completion, Delivery, Launch, and First and Last Light

[41] After completion of laboratory calibration, the  $M^3$  instrument was removed from the thermal-vacuum chamber and prepared for shipment to the ISRO Satellite Center (ISAC) in Bangalore, India. Figure 47 shows a picture of the  $M^3$  instrument with the opto-mechanical subsystem, passive radiator, cables, and electronics box on an optical bench prior to packing. Immediately following laboratory calibration, a pre-ship review was held and completed successfully on the 3rd of May 2007. Preparations were made to package and deliver the instrument along with required ground support equipment for spacecraft integration.  $M^3$  was shipped from Los Angeles International Airport on the 4 of August 2007 via Singapore Airlines Cargo Inc. to Bangalore India with one stop in Brussels, Belgium. Companion temperature and acceleration measurement as well as the JPL escort indicated no anomalies during transport. Once at ISAC,  $M^3$  was tested to confirm basic functionality and then stored in the shipping container under a clean, dry nitrogen purge. During the remainder of 2007 and first half of 2008, assembly continued on the Chandrayaan-1 spacecraft. During this period,  $M^3$  was attached to the anti-sun side

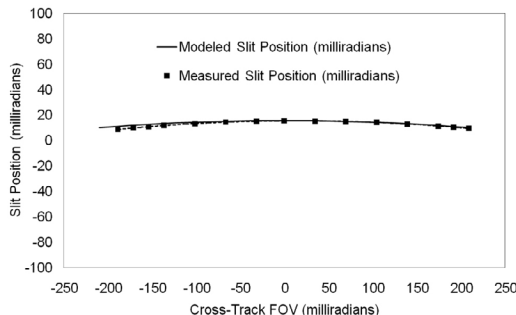


**Figure 46.**  $M^3$  projected slit function for the instrument camera model. The position of the slit varies by 7 milliradians over the  $\pm 209$  milliradian FOV of  $M^3$ . This function is used as part of the orthorectification process that projects the measured spectra onto the topographically varying surface of the Moon.

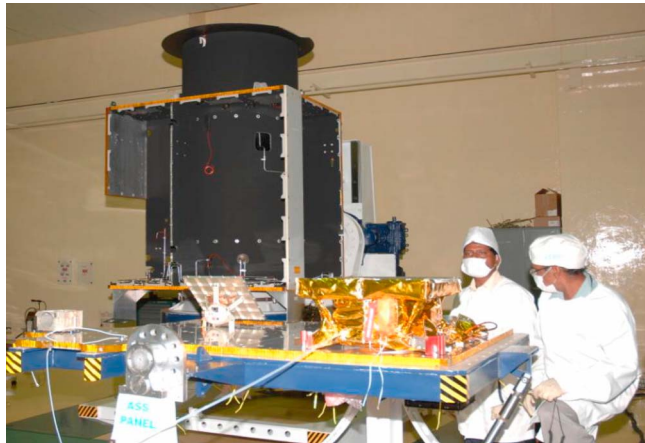


**Figure 48.** M<sup>3</sup> imaging spectrometer mounted on the anti-sun side panel of the Chandrayaan-1 spacecraft at ISRO ISAC.

panel of Chandrayaan-1 and power and data cables were connected as shown in Figure 48. Tests were performed to confirm M<sup>3</sup> operability with Chandrayaan-1. Signals from the M<sup>3</sup> detector array were recorded to verify full signal chain functionality. Even at room temperature some of the M<sup>3</sup> detector array elements provided non-saturated values. These detector values were verified with respect to those measured under room temperature conditions at the Jet Propulsion Laboratory during laboratory testing. When not installed on the spacecraft the M<sup>3</sup> instrument was maintained in the shipping container under clean dry nitrogen purge. In the summer of 2008 the Chandrayaan-1 spacecraft was completed with all 12 instruments installed. The spacecraft was transported to the launch facilities at Sriharikota to the north of Chennai on the eastern coast of India. Figure 49 shows the completed Chandrayaan-1 spacecraft with the M<sup>3</sup> instrument prior to launch. Chandrayaan-1 was integrated with the Indian Polar Satellite Launch Vehicle (PSLV) and prepared for launch in October of 2008.

[42] On the 22nd of October 2008, Chandrayaan-1 was launched successfully within a narrow weather window as shown in Figure 50. Soon after launch, while in Earth orbit, nominal spacecraft power and communication functions were confirmed. The M<sup>3</sup> instrument was maintained in survival and decontamination mode for transit to the Moon. Following a series five Earth orbit maneuvers over several days, the Chandrayaan-1 orbit was extended to a lunar transfer trajectory. On November 8th, a lunar orbit insertion maneuver was completed successfully. Over the following several days, a series of 4 lunar orbit maneuvers were completed to place Chandrayaan-1 in the nominal 100 km inertially fixed polar orbit on the 12th of November 2008. Soon after arrival in the nominal orbit, the Moon Impact Probe (MIP) payload was released successfully and commissioning of the remaining payloads began.

[43] On the 18th of November 2008 the M<sup>3</sup> imaging spectrometer was switched to engineering mode and the detector allowed to cool toward operational temperatures. This was the first time the M<sup>3</sup> detector array and spectrometer had been cooled since completion of laboratory

calibration in April of 2007. On the 19th of November, before the detector had fully cooled, the first light Global Mode image and spectra from the M<sup>3</sup> imaging spectrometer was acquired and is shown in image cube format in Figure 51. This is a portion of Harpalus Crater located near 52° 36' North latitude and 43° 24' West longitude. This first light Global Mode image and spectra demonstrated that the basic capabilities of the M<sup>3</sup> imaging spectrometer were in place and healthy onboard Chandrayaan-1 in orbit around the Moon. Global Mode measurements were planned to be acquired as long strips from the lunar pole to 55° in the opposite hemisphere such that consecutive acquisitions provide overlapping coverage. In a nominal M<sup>3</sup> image acquisition sequence, a companion short duration dark signal image is measured from the preceding non-illuminated portion of the orbit. These dark signal images provide the offset correction and a basis for assessing anomalous detector elements for each of the corresponding illuminated images. For example, Figure 52 shows the full data set acquisition, the Harpalus portion, and a zoom of the central peaks of Harpalus. Also on the 19th of November a first light Target Mode data set was acquired near longitude 43° west and latitude 53° north with a 68° solar illumination zenith angle. The image and example spectra from this data set are shown in Figure 53. While the solar illumination conditions were unfavorable and the detector was not at nominal cold operational temperature, these measurements confirmed that M<sup>3</sup> Target Mode was functional on board Chandrayaan-1 in addition to Global Mode.



**Figure 49.** Complete Chandrayaan-1 spacecraft with 12 payload elements including M<sup>3</sup> mounted on the anti-sun side panel.



**Figure 50.** Launch of Chandrayaan-1 on the 22nd of October 2008 with 12 science payloads including the M<sup>3</sup> imaging spectrometer.

[44] Soon after confirmation of M<sup>3</sup> on-orbit functionality, mission concerns arose due to the higher than expected temperatures throughout the spacecraft. Operational plans were adjusted to optimize the temperature environment of the spacecraft and instruments. These adjustments shifted much of the M<sup>3</sup> data acquisition to higher than planned solar beta angles and led to a more varied image data acquisition scenario. The beta angle is the angle between the spacecraft orbital plane and the sun, and for M<sup>3</sup> is related to the solar zenith angle at the equator for a given orbit. Due to these mission operation adjustments, far fewer M<sup>3</sup> data sets were collected through December and early January than planned. While these data sets had smaller solar beta angles and zenith angles at the equator, the detector temperatures were well above the nominal 156 K. Also in this period, on the 18th of December, the Chandrayaan-1 spacecraft performed a 180° yaw maneuver at beta angle 0 to maintain the anti-sun side panel on the anti-sun side of the spacecraft. This period from November 2008 through early January 2009 was designated optical period 1a (OP1a). The OP1a type designations were used by the M<sup>3</sup> team to track different

sets of data acquisition over the course of the mission [Boardman et al., 2011].

[45] A test Global Mode data set was acquired on the 25th of January with the M<sup>3</sup> detector at nominal operation temperature that included the Moscovense Basin on the lunar far side [Pieters et al., 2011]. Figure 54 shows a portion of this data set and a selected set of spectra that have been converted to apparent reflectance. The formula for calculating apparent surface reflectance is given in equation (1).

$$\rho_{ap}(\lambda) = \frac{L(\lambda)}{\cos(i) \times \frac{F_0(\lambda)}{\pi}} \times \left( \frac{1}{d_{AU}} \right)^2 \quad (1)$$

$\rho_{ap}$  is the apparent surface reflectance

$\lambda$  is wavelength

$L$  is the calibrated radiance measured by M<sup>3</sup>

$i$  is the solar zenith incidence angle

$F_0$  is the solar irradiance at one AU

$d_{AU}$  is the distance from surface to the sun in AU

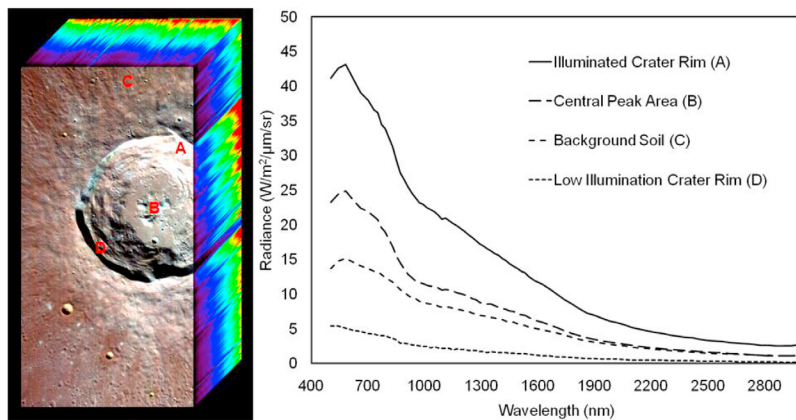


**Figure 51.** First light Global Mode image and spectra of Harpalus crater acquired by the M<sup>3</sup> imaging spectrometer on the 19th of November 2008. These spectra with calibration coefficients applied show that the full spectral range of M<sup>3</sup> was functioning even under these illumination conditions with a 61° solar zenith angle.

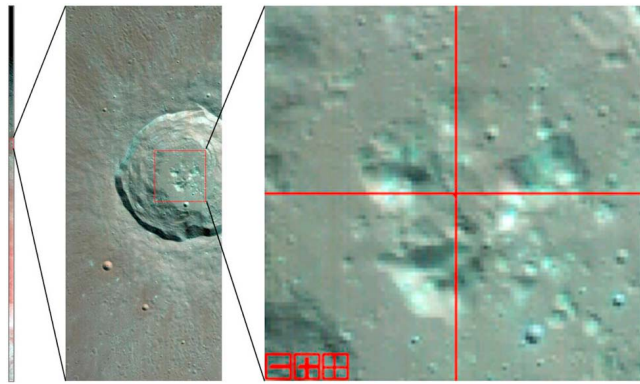


**Figure 52.** Example  $M^3$  Global Mode full data set acquisition that includes the Harpalus crater acquired on the 19th of November 2008. The left most image is the full data set acquired. The central image shows the Harpalus portion of the full image. To the right is a zoomed image of the central peaks of the crater.

[46] Conversion to apparent surface reflectance compensates for the solar irradiance spectrum, the solar incidence illumination angle, as well as solar distance and enhances the expression of mineral and compound absorption features in the measured spectra. In these spectra, 1 micron and 2 micron absorption features are evident as is a weak 3 micron absorption. The effect of temperature is also evident toward the long wavelength end of the spectrum with a rise in signal due to emitted energy. Early  $M^3$  measurement analysis of this type by the science team provided early evidence that the  $M^3$  imaging spectrometer was meeting the basic science measurement requirements necessary to achieve the full set of mission science goals and objective.

[47] Starting on January 31st a concerted  $M^3$  imaging campaign began that collected 382 illuminated and dark signal data sets through the 14th of February 2009. In this timeframe, designated optical period 1b (OP1b), a large fraction of the lunar surface was measured by  $M^3$  in Global Mode with illumination beta angles ranging from 43° to 57°. Optical period 2a (OP2a) commenced on the 15th of April 2009 at a beta angle of 60° and proceeded through the 27th

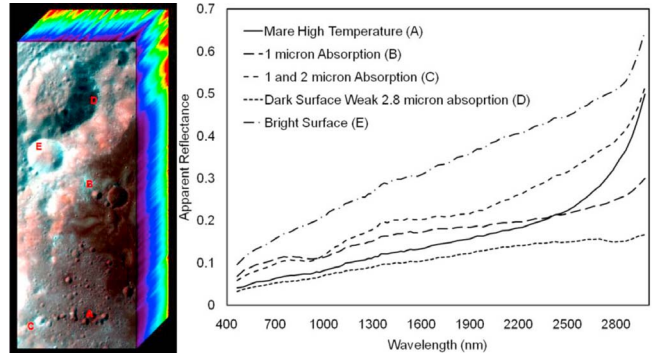


**Figure 54.**  $M^3$  Global Mode image and apparent surface reflectance spectra from a portion of the Moscoviene Basin on the far side of the Moon measured on the 25th of January 2009. These measurements were acquired with detector temperatures nominal detector temperatures ( $\leq 156$  K). A range of different spectral absorption features and temperature related effects are captured in the  $M^3$  spectra.

of April. A truncated optical period 2b (OP2b) began on the 13th of May and proceeded to the 16th of May. On the 19th of May 2009, for mission safety, the orbit of Chandrayaan-1 was raised from 100 km to 200 km.  $M^3$  imaging resumed imaging in optical period 2c (OP2c) on the 20th of May and proceeded through the 16th of August 2009. A second spacecraft 180° yaw maneuver was performed on the 18th of June to maintain the anti-sun side of the spacecraft. Figure 55 shows a plot through time of the  $M^3$  detector temperature and solar beta angle of the measured  $M^3$  data sets. with the optical periods delineated. In periods when the temperature was higher than nominal, the noise of the detector increased. At the higher beta angles, the corresponding surface solar zenith angles resulted in lower levels of illumination than planned, and increased abundance of shadows in the collected imaging spectrometer data sets. Even with measurements in off-nominal conditions, the signal-to-noise ratio of the measured data set supports the range of science goals and objectives of the  $M^3$  mission, although it does have adverse affects on data quality.

[48] On the 29th of August 2009 the Chandrayaan-1 flight mission ended with loss of communication with the space-

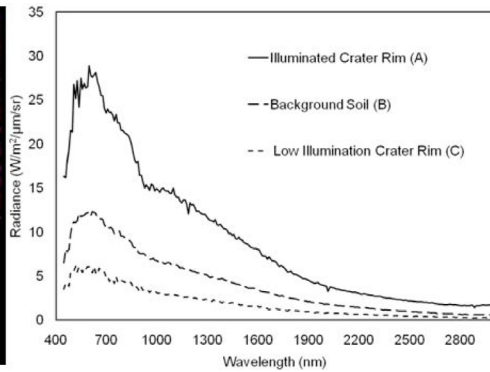
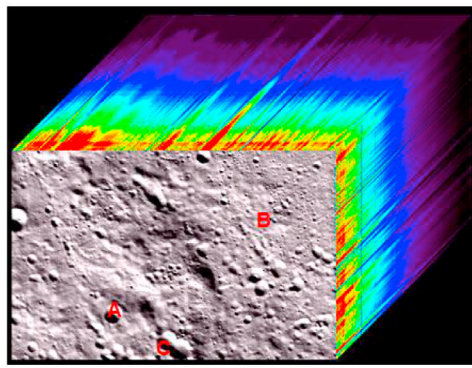


**Figure 53.**  $M^3$  Target Mode first light image with full spatial and spectral resolution acquired near longitude 136° west and latitude 63° north with a 68° zenith solar illumination angle. The spectra show above nominal noise because the detector was well above nominal temperature.

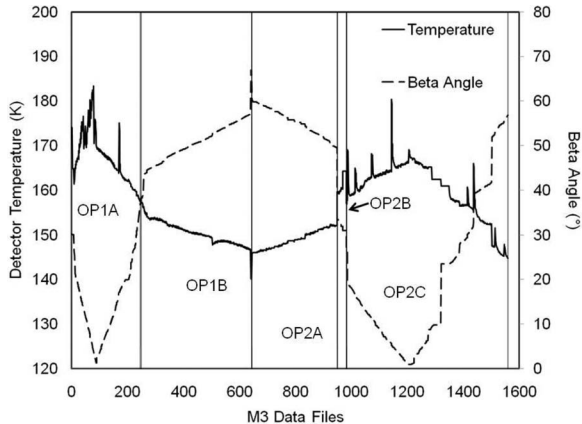


**Figure 55.** Plot of solar beta angle and M<sup>3</sup> detector temperature over life of the mission. The vertical lines separate the principal imaging periods.

craft. The last light image was acquired on the 16th of August 2009. A portion of the last light image includes Boyle crater near 52 south latitude and 178 east longitude and is shown in Figure 56. Over the course of the mission, M<sup>3</sup> downlinked a total of 1542 files consisting of 1386 Global Mode and 156 Target Mode data sets including both dark signal and illuminated surface images. From these down-linked data sets, 825 nominally illuminated Global Mode and 79 Target Mode images were acquired. 336 contiguous Global Mode images strips provide nearly full coverage of the lunar surface. The acquired M<sup>3</sup> measurements provide 95% complete Global Mode coverage of the Moon and meet the primary coverage requirements of the mission. These measurements are being used to address the full set of M<sup>3</sup> science goals and objectives. The Global Mode data set includes many areas with multiple acquisitions spanning a range of illumination angles that support photometric and temperature investigations. The Target Mode data sets acquired provide opportunities for science investigations using the full spectral and spatial resolutions of M<sup>3</sup> for selected areas of the Moon. The full operational orbital mission of M<sup>3</sup> occurred over the period between the 19th of November 2008 and the 29th of August 2009. The details of complete coverage acquisitions by M<sup>3</sup> over this period are described by *Boardman et al.* [2011].

## 7. Science Data Calibration

[49] Science data calibration is the process of applying and associating the full set of spectral, radiometric and spatial calibration factors to the M<sup>3</sup> imaging spectrometer down-linked measurements. For M<sup>3</sup>, calibration also includes suppression of known instrument artifacts to the extent feasible. Calibrated M<sup>3</sup> radiance measurements with associated observation and location parameters are designated Level 1b. For M<sup>3</sup> science data calibration, a sequence of processing algorithms are applied to transform the downlinked CCSDS format packets to Level 1b spectrally, radiometrically, and spatially calibrated science measurements. The format of the calibrated M<sup>3</sup> science data set is three-dimensional binary arrays with detached ASCII headers.

[50] The basic M<sup>3</sup> radiometric calibration algorithm that converts the measured raw 12 bit digitized numbers to units of spectral radiance for each line and sample in the image is given in equation (2). A series of correction algorithms that are described below are applied to compensate for a range of instrumental effects in the raw measurements.

$$L_{l,s,\lambda} = RCC_{\lambda} \left( C_{s,\lambda} \left( DN_{l,s,\lambda} - \overline{DS}_{s,\lambda} \right) \right). \quad (2)$$

$l$  is the measured image line

$s$  is the image cross-track sample

$\lambda$  is the spectral channel corresponding to wavelength

$L_{l,s,\lambda}$  are the calibration radiance values for every line, sample and wavelength

$RCC_{\lambda}$  are the laboratory radiometric calibration coefficients as a function of wavelength

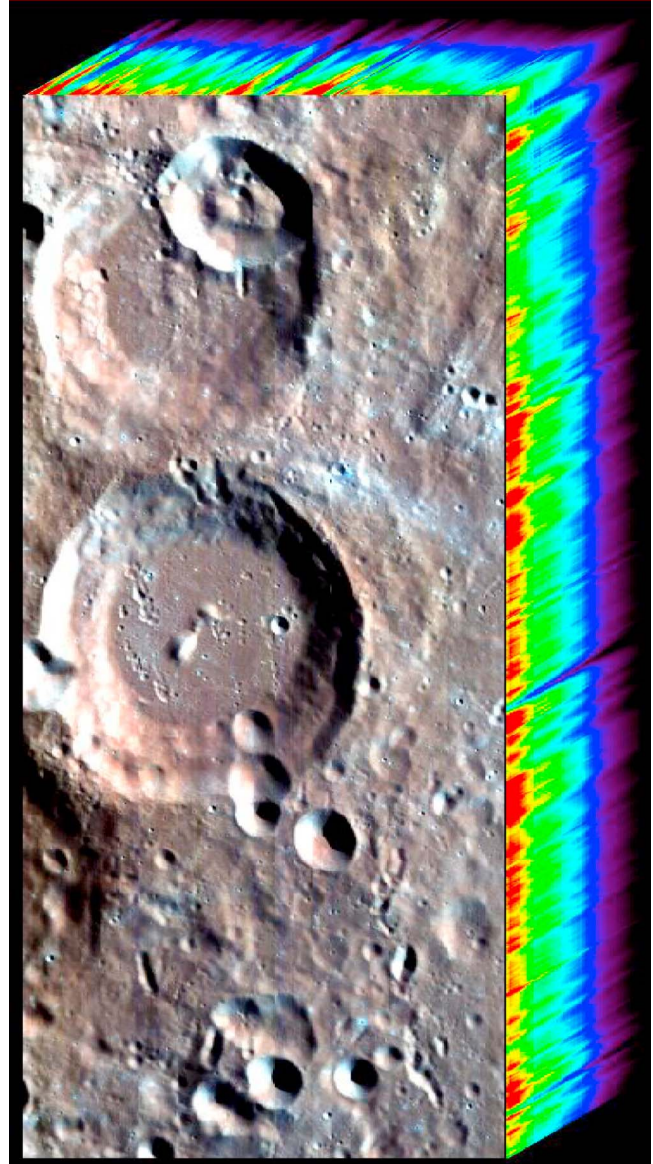


**Figure 56.** Last light image from the M<sup>3</sup> imaging spectrometer including Boyle crater acquired on the 16th of August 2009 near latitude 52 south and longitude 178 east.

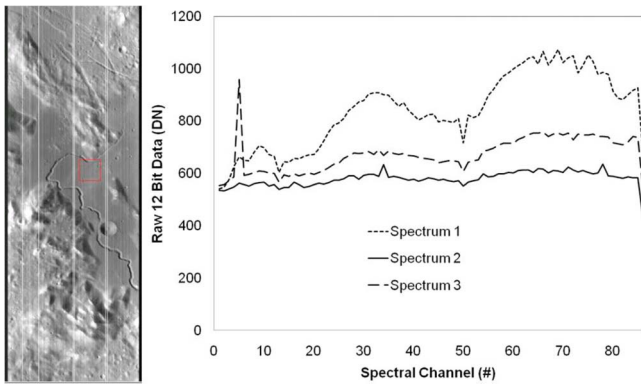


**Figure 57.** M<sup>3</sup> Global Mode Level 0 data acquired on the 5th of February 2009 from the Apollo 15 landing site after unpacking from CCSDS downlinked files. The image is from spectral channel 60. Vertical stripes are evident from the different gains, offset and performance of the instrument and detector array. The masked and vignetted edge elements of the detector array for dark signal and scattered light monitoring are evident. The image is transposed left to right due to the yaw rotation state of Chandrayaan-1 in this portion of the mission. The three Level 0 spectra show the uncompensated throughput and offset of the end-to-end M<sup>3</sup> instrument system. An anomalous detector spike is present at channel 5 in spectrum 2. Lower signal level at the order sorting filter seams occurs at channel 13 and 50.

$C_{s,\lambda}$  encompasses the correction algorithms and factors described below that compensate for: anomalous detector elements, dark pedestal shift, electronic panel ghost, non linearity, laboratory scattered light, flat field, and image based flat field.

$DN_{l,s,\lambda}$  are the 12-bit digitized numbers recorded by the M<sup>3</sup> instrument

$\overline{DS}_{s,\lambda}$  are the average dark signal image values associated with the corresponding illuminated image.

[51] The M<sup>3</sup> calibration sequence begins with unpacking the downlinked CCSDS packets to generate a lossless compressed file. This file is uncompressed from the Level 0 image with lines, samples and spectral channels. Figure 57 shows a portion of a Level 0 Global Mode image including the Apollo 15 landing site and Hadley Rille that was acquired on the 5th of February 2009. The vertical stripes in the image result from variability of the gains, offsets and performance of different elements of the detector array. The consistent vertical stripes at cross-track samples 81, 161 and 241 are related to uncompensated electronic signal chain effects associated with readout of the four panels of the detector array. The masked and vignetted regions of the left and right side of the image that are used to monitor dark signal levels and scattered light are evident. This level 0 image is transposed left to right due to the yaw state of the Chandrayaan-1 spacecraft during this portion of the mission. Correction to nominal left right and North up is performed in the final step of the level 1b science data calibration. Three Level 0 spectra extracted from this image are shown. The signal levels in these spectra are a function of the reflected and emitted energy from the surface plus the full set of instrument throughputs, offsets, and other properties. A

significant detector spike is evident at channel 5 in spectrum 2 and an example of one of the anomalous detector elements in this HgCdTe detector array. Reduced throughput due to the order sorting filter seam is present at channels 13 and 50 of this Global Mode data set.

[52] Following unpacking of the CCSDS downlinked data set, the dark signal levels are calculated and subtracted. For all nominally acquired M<sup>3</sup> data sets, a dark signal image data set is acquired at high latitude on the non-illuminated side of the Moon prior to acquisition of the illuminated data set. This dark signal data set is averaged for all lines to generate an average dark signal with one value for each cross-track sample and spectral channel. An array of 640 by 260 real dark signal values is generated for Target Mode, and 320 by 86 for Global Mode. This dark signal average is subtracted from each cross-track sample and spectral channel for all lines in the corresponding illuminated image of the Moon. In cases where a dark signal image was not successfully acquired, the dark signal image acquired nearest in time is used. Figure 58 shows the dark signal corrected image and the corresponding Level 0 spectra from the Apollo 15 example data set. Dark signal correction removes the overall instrument related dark signal levels and corrects detector to detector offset differences. In this case the anomalous spike in spectrum 2 was in the dark signal level and has been compensated with dark signal correction.

[53] Identification and correction of anomalous detector elements follows dark signal level correction in the calibration processing system. M<sup>3</sup> uses 260 by 640 detector elements of the 6604a HgTeCd detector array for a total of 166400 elements. With this detector material and the 3000 nm upper wavelength limit, a number of the detector elements exhibit non standard performance. Anomalous detector elements are defined as either non-responsive, fixed high signal, or excessively noisy. Variability in the number of anomalous detector array elements for a given image acquisition is largely a function of the detector array temperature. Because the M<sup>3</sup> detector array temperature varied significantly through the optical periods during the Chandrayaan-1 mission, the anomalous detector elements are identified for each image data set based on the statistics

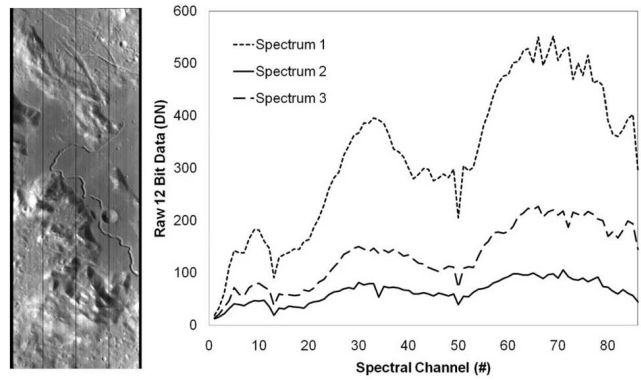


**Figure 58.** Dark signal corrected channel 60 image of the Apollo 15 landing site area. The instrument dark signal level and detector to detector offsets have been compensated. M<sup>3</sup> Global Mode Level 0 spectra after dark signal correction for the Apollo 15 landing site area.

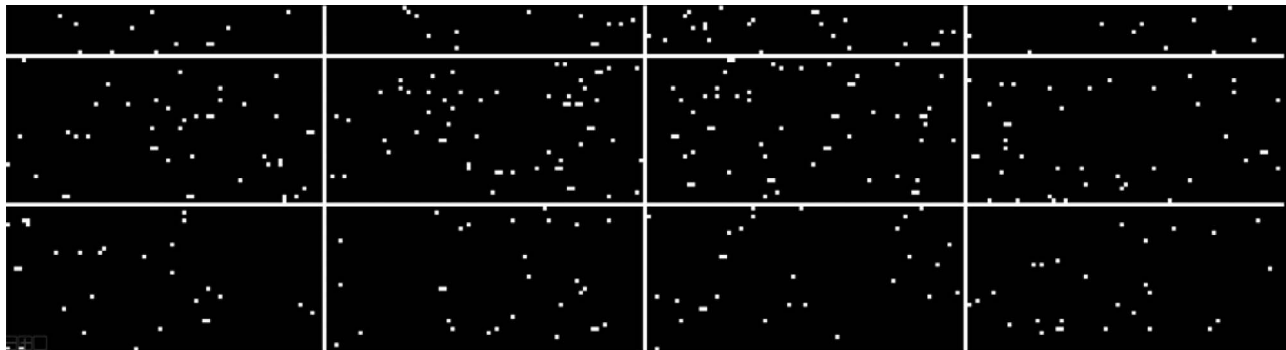


**Figure 59.**  $M^3$  Global Mode anomalous detector element image for the Apollo 15 landing site image. Detector elements with high, low or excessively variable signal are designated along with the detector panel boundary columns and filter seam rows.

of the associated dark signal image. For Global Mode, detector elements are designated as anomalous if the average digitized dark signal is above 1000 DN or below 300 DN or the standard deviation is above 2.5 DN. For Target Mode, anomalous detector elements are designated when the dark signal values are above 1000 DN below 300 DN or have a standard deviation above 5.0 DN. Nominal dark signal levels are 500 DN for Global and Target Mode. These thresholds were determined through analysis of the full set of dark signal images acquired on orbit for both Global Mode and Target Mode. From these threshold levels, an anomalous detector element image is generated with dimensions equal to the number of cross-track samples and spectral channels. Figure 59 shows the anomalous detector element image for the Apollo 15 landing site data set. In this image, cross-track samples 81, 161 and 241, which are the detector panel boundaries, are included, as are spectral channels 13 and 50, which are the locations of the filter seams. For Target Mode data, the corresponding detector panel boundaries are at cross-track sample 161, 321, and 481 and the filter seams are at spectral channel 41, 42 and 116. As part of this step in the processing sequence these anomalous detector elements are interpolated in the illuminated image. Simple linear interpolation is applied in the spectral direction except for the fixed column anomalies of the detector panel boundaries where cross-track interpolation is used.

[54] The next step in the science data calibration processing sequence is correction for the dark pedestal shift that is shown to occur in the detector array signal chain. Dark pedestal shift is expressed as a small proportional drop in the dark signal level for the detector row when the detector row is illuminated. This effect is captured by the set of dark masked detector array elements in Target Mode cross-track columns 1–8 and 637–640. An empirical function has been developed to estimate the dark pedestal shift based upon the signal in the illuminated portion of the array relative to the signal in these dark masked detector elements. This correction is applied to all samples in the image on a line by line basis.

[55] Suppression of a weak electronic panel ghost effect follows correction for the dark pedestal shift. The  $M^3$  6604a detector array signal chain is read out through the four outputs corresponding to the four 160-pixel wide panels of the 640-pixel wide detector array. In this readout process, a

strong signal in one panel generates a weak (<1%) negative electronic ghost in the other three detector panels. For example, in Target Mode, if a bright signal is present at cross-track sample 50, as small negative signal will be imparted in the other three detector zones at sample 160 + 50, 320 + 50 and 480 + 50. This phenomenon is also observed in the CRISM and MaRS imaging spectrometers. The strength of the ghost was assessed empirically based on laboratory and on-orbit measurements. A simple fractional correction processing step is applied to the image following correction of anomalous detector elements to suppress this electronic panel ghost artifact.

[56] A nonlinearity correction algorithm has been developed for the  $M^3$  data based upon the linearity measurements acquired in the laboratory and implemented with a finely interpolated look-up-table algorithm that enables rapid nonlinearity compensation in the processing system.

[57] Scattered light effects are assessed and suppressed in the next step in the  $M^3$  science data calibration processing system.  $M^3$  was designed with columns of detector elements that are nominally vigneted by the spectrometer slit. Signal arriving at these detectors provides an estimate of the background scattered light. These vigneted detector element columns correspond to Target Mode samples 9–15 and 628–636. Using laboratory and on-orbit measurements from these vigneted detector array columns, a scattered light correction function has been developed to estimate the scattered light based upon the signal distribution in the illuminated portion of the array. This additive correction is applied to the image on a line by line basis to provide a background scattered light correction. At present, this is a simple first order scattered light correction. As the  $M^3$  science data calibration processing sequence is refined and updated, further work is expected to refine the suppression of scattered light.

[58] Laboratory flat field correction is the next step in the  $M^3$  science data calibration processing sequence. When illuminated by a uniform light source, there is variability in the cross-track radiometric response of the 6604a detector array elements as well as the reflective and transmissive components of the full  $M^3$  instrument system. In the laboratory, a flat field image was calculated to account for this variability and is shown in Figure 39. The flat field image is 640 spatial by 260 spectral values for Target Mode and 320 spatial by 86 spectral values for Global Mode. In this

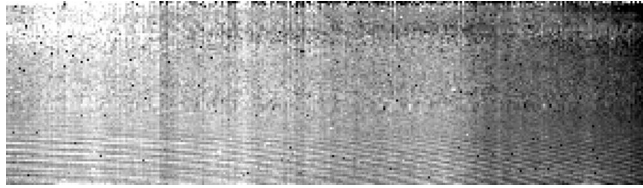


**Figure 60.** Simple image based flat field that shows strong cross-track gradient due to lunar surface photometry and vertical stripes due to residual lunar surface cross-track brightness variation.

processing step, the flat field is multiplied by the image to compensate for the laboratory-determined radiometric response variability in the full system.

[59] Once in orbit around the Moon, an assessment of the flat field correction was made by averaging long orbital data sets and developing simple image-based flat field images. Analysis of these on-orbit flat field images showed significant residual variability in the  $M^3$  detector response and instrument throughput that were not compensated by the laboratory flat field. The variability is hypothesized to result in large part from the wider than expected range of temperatures experienced on orbit. Based on these analyses, the necessity of an additional image-based flat field correction was established. The image-based flat field correction values were derived by averaging the longest on orbit data sets and then dividing by the average of the central 40 cross-track sample values. Figure 60 shows the simple image based flat field for the Apollo 15 landing site image shown earlier. The long wavelength ripple in this flat field is attributed to a subtle etalon effect between the detector array and order sorting filter. Use of this simple initial image based flat field suppressed many of the residual effects not compensated by the laboratory flat field. However, with this flat field both cross-track gradients due to surface photometry and vertical stripes due to variability in cross-track surface brightness are present. Use of this simple image-based flat field inappropriately suppressed the cross-track photometry and introduced erroneous vertical striping. To avoid these undesirable effects, an enhanced methodology was developed where a two-dimensional surface is fit to the image based flat field and removed from the flat field correction factor. To suppress the impact of major features in the image-based flat field on the resulting illuminated lunar surface images, a smoothed spectral average is divided out in a final flat field. Figure 61 shows the enhanced image-based flat field correction for the Apollo 15 landing site. This flat field

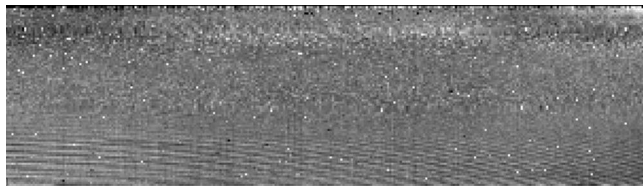


**Figure 61.** Optimized  $M^3$  science data calibration image based flat field required to suppress on-orbit  $M^3$  instrument variability associated with changing thermal environment. The dominant effects suppressed are detector to detector variability and long wavelength ripple.

captures the instrumental responsivity variability with little evidence of residual photometric effects or surface structure. In the  $M^3$  science data calibration processing chain, such enhanced image-based flat fields are applied to suppress detector and instrument throughput response variability that is not compensated by the laboratory flat field correction.

[60] Following the full suite of pre-processing steps in the  $M^3$  science data calibration sequence, the resulting image is multiplied by the laboratory-traced radiometric calibration coefficients that convert the corrected digitized values to units of radiance ( $\text{W}/\text{m}^2/\text{nm}/\text{sr}$ ). When the calibrated image is generated, only the illuminated cross-track elements are preserved in the calibrated image file. At this step in the processing system the orientation of the downlink file is flipped so that north is the first image line and west is the first image sample. This is required due to the rotation of the spacecraft at beta angle  $0^\circ$  and the orbit illumination for the specific optical period. For Global Mode spectral channel 2 to 86 and for Target Mode channels 5 to 260 are preserved. Channel 1 in Global Mode and Channels 1 to 4 in Target Mode were found to have consistently low signal and an excessive amount of scattered light, and were omitted from the calibrated products. In this calibration processing step, the laboratory spectral calibration values for spectral channel position and FWHM are associated with the image. Figure 62 shows the calibrated Apollo 15 landing site image and corresponding example spectra in radiance units versus wavelength. As part of the Level 1b calibration the spatial calibration data sets are associated with the spectral and radiometrically calibrated data. These spatial calibration data sets describe the location and observation properties of the measurements. The location file provides the latitude and longitude and elevation of every spectrum. The observation file provides the illumination, and observation angles of every spectrum are provided along with the surface slope and aspect angles. Further details regarding the contents and generation of these location and observation files are provided by *Boardman et al.* [2011]. These files have a one-to-one mapping with the calibrated spectral image files and are provided to support science analysis of the Moon with the measured  $M^3$  spectra.

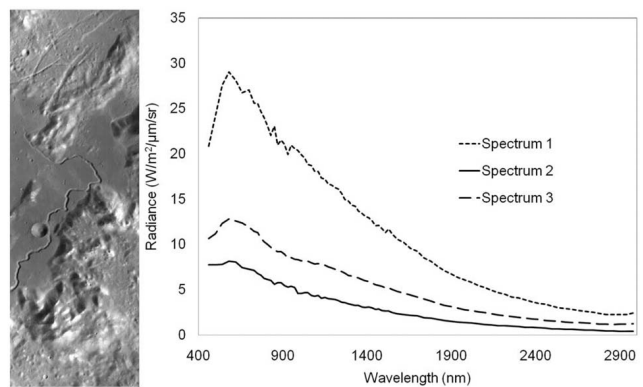


**Figure 62.** Calibrated  $M^3$  channel 60 image of the Apollo 15 landing site with all correction applied with example spectra over a range of radiance levels. Some variation is present in the spectrum near 900 nm due to low illumination and a slightly warm detector.

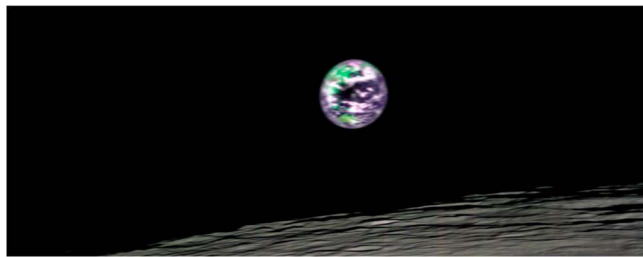


**Figure 63.**  $M^3$  measurement of the Earth from lunar orbit acquired on the 22nd of July 2009. The image include eastern Asia, Australia and the Pacific Ocean and was acquired during the passage of a solar eclipse of the Earth. The eclipse complicates use of these measurements for estimation of Earth hemispherical spectral flux values. The Earth spans approximately 40  $M^3$  Global Mode spatial samples in the cross-track direction. The lunar limb is captured in lower portion of the image.

[61] The  $M^3$  science data calibration processing system has been developed based upon the high uniformity broad spectral range pushbroom design characteristics of the  $M^3$  imaging spectrometer in conjunction with the laboratory characterization and calibration measurements. Based on analyses and investigations with the  $M^3$  science team, an image-based enhanced flat field correction has been added to suppress throughput and responsivity variability associated with the wider than expected temperature range experienced by  $M^3$  in lunar orbit. In the time since the initial  $M^3$  on orbit images were downlinked, various subsets of these processing steps have been applied to the downlinked measurements and used by the  $M^3$  science team. An early version of processing was designated “calibration-H” and included dark signal subtraction, anomalous detector correction, laboratory flat field, simple image-based flat field, and radiometric calibration. Version “calibration-K” added the enhanced image-based flat field correction. Version “calibration-R3” added dark pedestal shift correction, electronic panel ghost and refined image-based flat field correction. Version “calibration-R4” includes an update to the calibration of the long wavelength channels of  $M^3$ . The June 2010 delivery to the Planetary Data System (PDS) is “calibration-R3.” The December 2010 delivery is version “calibration-R4,” and replaces the June 2010 delivery. The non linearity correction is still in the process of validation and is expected to be included in the next update to the PDS. As enhanced calibration algorithms are identified by the  $M^3$  science team and others, the science data calibration processing system will be updated, tested, and the enhancements implemented and documented.

## 8. Validation of the on-Orbit Characteristics and Calibration

[62] Validation of the on-orbit spectral, radiometric, and spatial calibration and uniformity characteristics of the  $M^3$  imaging spectrometer is essential for use of the measurements at many levels. Characteristic and calibration validation supports direct science use of the  $M^3$  measurements as well as use of  $M^3$  measurements with physically based models and comparison of  $M^3$  measurements with mea-

surement by other instruments and laboratory analyses. For all of these reasons, validation of the on-orbit measurement characteristics and calibration of  $M^3$  has been a core focus of the  $M^3$  science team.

[63] On-orbit spectral calibration of  $M^3$  was initially validated with comparison of the location of broad spectral features such as the absorptions of pyroxene and olivine measured in the  $M^3$  spectra. A more precise validation of the spectral calibration was possible with the acquisition of an earth-view data set on the 22nd of July 2009. This image was acquired by pointing the Chandrayaan-1 spacecraft in the Earth direction and then sweeping the  $M^3$  pushbroom field-of-view across the Earth with a spacecraft pitch maneuver. Figure 63 shows an image of the Earth acquired in Global Mode with the lunar surface in the foreground. This data set includes the western Pacific region of the Earth and was acquired coincident with a solar eclipse in the center of the image. Major illuminated composition types include: ocean, land, vegetation, and clouds. A series of spectra extracted from this data set are shown in Figure 64. In these spectra, the strong atmospheric absorptions of water vapor are well expressed at 940, 1150, 1400, 1900 and 2600 nm. The 760 nm oxygen absorption is also identifiable. The MODTRAN [Berk et al., 1998, 1999] radiative transfer code was run for the general illumination and observation geometry of this acquisition with reflectance values simulating high reflectance clouds. A comparison of the  $M^3$  calibrated spectra and MODTRAN modeled spectra is given in Figure 65. The MODTRAN oxygen and water vapor absorption features are traced to the HITRAN database of atmospheric gas absorption lines. The  $M^3$  spectral calibration is traced to the laser calibration sphere with known laser wavelengths. The correspondence between the  $M^3$  and MODTRAN spectral absorption features provide an important on-orbit validation of the  $M^3$  spectral calibration.

[64] Radiometric calibration of  $M^3$  on-orbit was tested early through comparison of the shape of the Level 1b radiance with respect to modeled radiance spectra from sites of returned Apollo 16 soil samples. Considerable uncer-

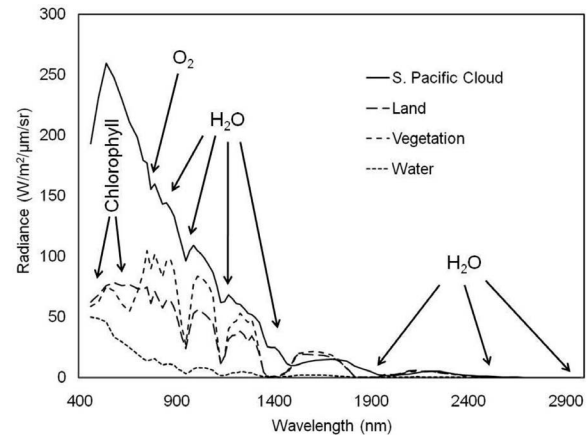


**Figure 64.**  $M^3$  spectra of the Earth acquired from lunar orbit on the 22nd of July 2009. Spectra from vegetation with the chlorophyll absorption as well as spectra from cloud, land and water areas are shown. The oxygen and water vapor absorption features of the atmosphere provide a basis for assessing the on-orbit spectral calibration of  $M^3$ .

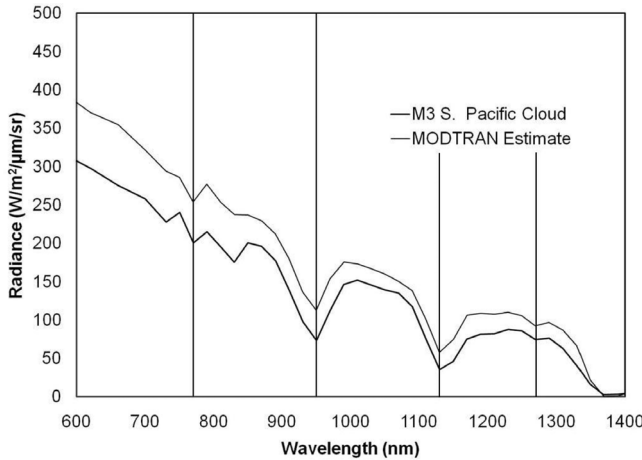


**Figure 65.** Comparison of a  $M^3$  calibrated spectrum of the Earth measured from lunar orbit with a MODTRAN modeled spectrum with the same illumination and observation geometry and cloud like reflectance. The close correspondence between absorption features of the measured and modeled spectra provide an on-orbit validation of the  $M^3$  spectral calibration.

tainty in this technique arises from the disturbance of the soil in the process of collection and transport and preparation for measurement in terrestrial laboratories. Additional uncertainty is accrued due to the variation in scale between the soil sample and the  $M^3$  spatial sampling distance of nominally 70 m for Target Mode and 140 m for Global Mode. The Apollo 16 landing site image used to evaluate the  $M^3$  radiometric calibration was acquired on the 8th of January 2009, with a solar zenith angle of  $23^\circ$ . The radiance from this area was modeled from the mature Apollo 16 soil (#62231) laboratory spectrum and the MODTRAN irradiance spectrum for the  $23^\circ$  zenith angle. The measured spectrum was extracted from the  $M^3$  data set. Figure 66 shows a comparison between the modeled spectrum and

the  $M^3$  measurement of the Apollo 16 ground calibration site. There is an overall correspondence in shape but a significant difference in absolute radiance levels, which is attributed largely to differences in disturbance, scale, location, illumination and temperature. For equivalent on-orbit calibration validation on Earth, more than 1000 in situ ground reflectance measurements are acquired concurrently with exact matching between the spaceborne and ground sampled areas [Green et al., 2003]. An enhanced radiometric calibration validation effort was pursued through comparison of the  $M^3$  measurements with measurements from the United States Geological Survey RObotic Lunar Observatory (ROLO) [Kieffer and Wildey, 1996; Stone and Kieffer, 2002]. The  $M^3$  data set was searched for measurements with similar observation geometries to those achieved with ROLO. A good match was found near Mare Serenitatis. For this comparison both the  $M^3$  and ROLO measurements are converted to apparent reflectance as described previously. A comparison of the  $M^3$  and ROLO apparent reflectance measurements for this site are given in Figure 67. Good agreement is evident in the spectral range covered by these measurements and is considered good initial validation of the  $M^3$  on-orbit radiometric calibration. Radiometric calibration validation activities will continue with future analyses and inter-comparison activities with measurements of the Moon by instruments on other missions. An important remaining challenge will be the need for comparison measurements acquired with very similar illumination and observational conditions. Work remains to compare  $M^3$  observations with other lunar observing satellites including those in Earth orbit.

[65] On-orbit noise was validated by calculating the standard deviation of the dark signal images acquired in association with each illuminated image. Figure 68 shows the noise frequency distribution and cumulative frequency distribution for the Target Mode dark signal measurement acquired on the 25th of January 2009 at 155 K. The median value is 0.66 DN and 90% of the values fall below 0.86 DN. These values are in good agreement with the laboratory

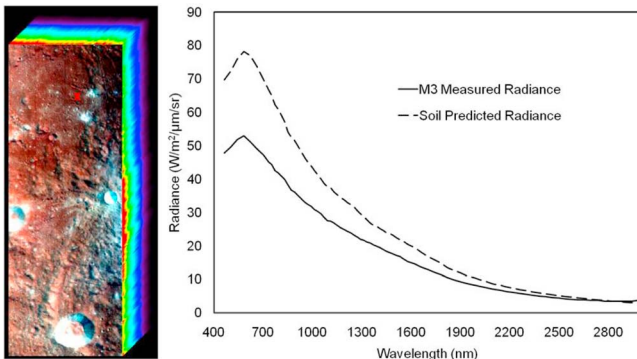


**Figure 66.** Apollo 16 landing site measured by  $M^3$  on the 8th of January 2009. The reflectance measured of the returned Apollo 16 soil sample #62231 has been used to estimate the radiance from the nominal calibration site in the image. Difference is the sample scale, sample location and illumination geometries, temperature as well as disturbance of the soil contribute to the difference in the modeled and measured spectrum.

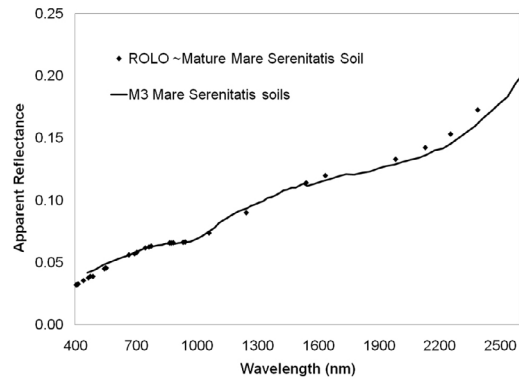


**Figure 67.** Comparison of  $M^3$  calibrated spectra that have been converted to apparent reflectance from Mare Serenitatis with measurements from ROLO with comparable illumination and observation conditions. The  $M^3$  measurements were collected with a  $29^\circ$  zenith angle and near  $0^\circ$  observation angle. The ROLO measurements were acquire with an illumination of  $23^\circ$  and observation angle of  $26^\circ$  and have been adjusted to a  $30^\circ$  phase for comparison with  $M^3$ .

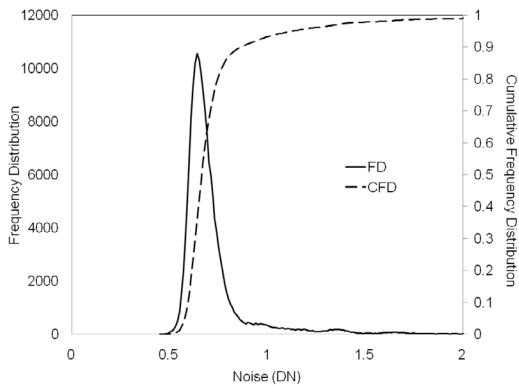


**Figure 68.**  $M^3$  on-orbit noise validation calculated at the distribution of the standard deviation from the dark signal measurements acquired on the 25th of January 2009 in Target Mode.

noise measurement of 0.68 DN and 0.87 DN from dark signal measurements acquired at 155 K acquired on the 29th of April of 2007 during laboratory characterization and calibration. This validates the noise performance of  $M^3$  in the lunar orbital environment for the planned operation temperature. Noise values higher and lower than this were recorded in the full  $M^3$  data set due principally to the variation in detector array and spectrometer temperature associated with the thermal anomalies encountered throughout the mission.

[66] Initial validation of  $M^3$ 's spatial characteristics is provided by examining the spatial detail of the returned  $M^3$  imaging spectrometer images. Comparison of the spatial content of  $M^3$  images with images acquired by the Clementine Mission provides a key validation that  $M^3$  has achieved significantly finer spatial resolution than other measurements from lunar orbit. Figure 69 shows a comparison of a Clementine image and an  $M^3$  Global Mode image for the Harpalus crater. The  $M^3$  image provides significantly finer detail even in this Global Mode data set with nominally 140 m spatial sampling. Cross-comparisons between  $M^3$

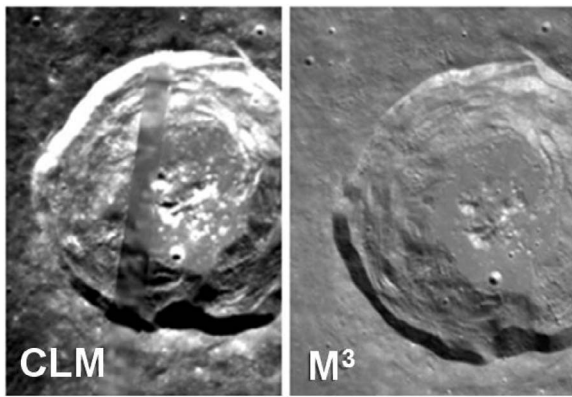


**Figure 69.** Comparison of  $M^3$  Global Mode spatial measurements over Harpalus crater acquired on the 19th of November 2008 with measurements acquired by the Clementine mission. Even with the 140 m sampling of  $M^3$  in Global Mode, considerably finer detail is preserved in the  $M^3$  image.

and Clementine are described in greater detail by Kramer et al. [2011]. The 24 degree field of view has been validated with the on-orbit spatial and geometric analyses described by Boardman et al. [2011]. With 608 illuminated cross-track samples measured in Target Mode, the cross-track sampling is 0.69 milliradians. The Global Mode cross-track sampling with 304 samples is 1.38 milliradians. The along-track spatial sampling is defined by the image line measurement rate of 0.025 s for Global Mode and 0.05 s for Target Mode. These along-track sampling intervals are validated on-orbit with the time tags provided with the downlinked data. Future spatial characteristic validation will proceed with comparison to and analysis with new high spatial resolution data sets acquired by the Kaguya (Selene) and LRO missions.

[67] Validation of spectral cross-track uniformity has been investigated with the Earth view data set acquired on the 22nd of July 2009. In this data set the Chandrayaan-1 spacecraft pointed  $M^3$  at the Earth and performed a pitch maneuver to acquire images with the Earth in the center of the  $M^3$  FOV. The Earth occupies 27 cross-track samples in Global Mode when viewed by  $M^3$  from lunar orbit<sup>5</sup>. The Earth measurement maneuver was repeated 9 times on this date. Variation of the position of the Earth in the  $M^3$  imaging spectrometer FOV across this sequence of measurements allowed sampling of atmospheric absorption feature in areas of bright clouds in different parts of the  $M^3$  FOV. The positions of usable cloud spectra of the Earth ranged from cross-track sample 131 to 230. This spans 100 samples of the nominally 304 cross-track samples of  $M^3$  Global Mode. Figure 70 shows the extracted cloud spectra from these samples that include atmospheric absorption features from water vapor and oxygen. Because the spectra were necessarily extracted from different times and different portions of the Earth to span the largest amount of the FOV possible, the cloud and atmosphere components are not identical. This causes variation in the intensity of the radiance signal and strength of the atmospheric features. However, even with this caveat, the alignment of the water vapor and oxygen absorption features in this portion of the spectrum provides validation of the cross-track spectral uniformity of the  $M^3$  instrument in lunar orbit. Cross-track

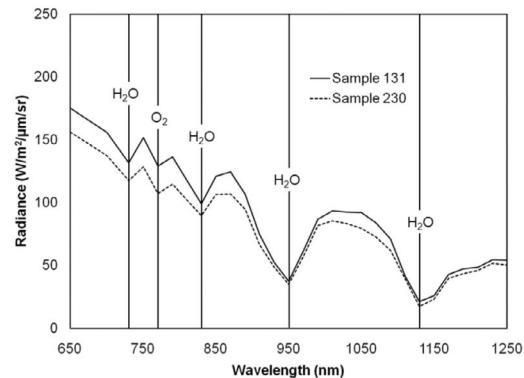


**Figure 70.** Comparison of Earth cloud spectra from Global Mode cross-track samples 131 and 230 showing excellent cross-track spectral alignment uniformity. These measurements provide validation of the  $M^3$  cross-track spectral uniformity while in lunar orbit.

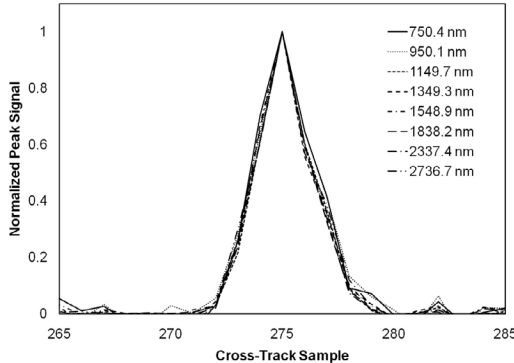


**Figure 71.** Normalized cross-track profiles across a isolated bright sample for a range of  $M^3$  Global Mode wavelengths. The close alignment of the cross-track profiles spanning this wide wavelength range provides validation of the  $M^3$  imaging spectrometer spectral IFOV uniformity in the orbital environment of the Moon.

spectral uniformity is one of the key science requirements and design characteristics of the  $M^3$  imaging spectrometer.

[68] A second key science requirement and design characteristic of  $M^3$  is the spectral IFOV uniformity that describes the position of the IFOV with respect to wavelength. Assessment of this property was pursued by analyzing isolated bright targets in the dominantly shadowed polar regions of the  $M^3$  data sets. Figure 71 show a series of Global Mode cross-track profiles for different wavelengths spanning the  $M^3$  spectral range from 750.4 to 2736.7 nm. These cross-track profiles were extracted from a data set acquired on the 25th of January 2009 at  $88^\circ$  North latitude with a solar zenith angle of  $88.5^\circ$ . These profiles cross a small illuminated peak in the otherwise shadowed polar region. Each of the profiles has been normalized to the high radiance value. The alignment of these normalized profiles from different spectral regions as they cross the bright illuminated sample provides validation of the spectral IFOV uniformity of the  $M^3$  imaging spectrometer in the orbital environment around the Moon.

[69] An understanding of the validity of the spectral, radiometric, spatial and uniformity characteristics while in orbit around the Moon is essential for all scientific investigations that utilize  $M^3$  measurements. A series of analyses have been pursued with measurements acquired in lunar orbit to validate the on-orbit spectral, radiometric, spatial, and uniformity characteristics. The assessments presented here have been necessarily limited by the data sets available for validation. For example, unlike the Earth, extensive independent in situ measurements of the surface reflectance properties of the Moon do not exist. However, within the existing constraints the analyses presented here show good initial validation of the spectral, radiometric, spatial and uniformity measurement characteristics of  $M^3$  in orbit and support use of  $M^3$  imaging spectrometer measurements for lunar science initiatives.

## 9. Summary and Conclusions

[70] A specific set of science and exploration science goals and objectives were established for the proposed Discovery

Moon Mineralogy Mapper mission. These goals and objectives required measurement of the Moon's surface composition with unprecedented specificity, at fine spatial scale, and over more than 90% of the surface. To pursue this science a high uniformity and high SNR imaging spectrometer was designed that was also low mass, low power, and compact in volume. The  $M^3$  imaging spectrometer required use of several enabling elements that had previously never been flown in space. These included an optimized high uniformity Offner design, the extended spectral range HgCdTe detector array (430 to 3000 nm), the new parabolic reflector passive radiator cooler, and efficiency-tuned, multifacet, convex, electron-beam lithography diffraction grating, and submicron adjustable component mounts lockable for spaceflight. All of these elements were successfully integrated into the  $M^3$  design to enable the full set of science measurement requirements.

[71] Following selection in February 2005, the  $M^3$  imaging spectrometer instrument was principally developed over a period of 24 Months starting from May 2005 when significant funds where accessible. Development proceed from system requirements review to preliminary design review and critical design review in quick succession. With this rapid development schedule the first spectrum was acquired on the 15th of December 2006 and full instrument assembly and alignment was completed by the end of March 2007. The high uniformity alignment requirements of >90% spectral cross-track uniformity and >90% spectral IFOV uniformity were achieved for the first time for a space-borne pushbroom imaging spectrometer. The  $M^3$  instrument was spectrally, radiometrically, and spatially characterized and calibrated in the laboratory in the Month of April 2007. These calibration measurements were rapidly analyzed and were used in conjunction with the full suite of instrument development documentation and analyses to support a pre-ship review.  $M^3$  passed the pre-ship review on the 3rd of May 2007. In early August 2007,  $M^3$  was shipped for integration with the spacecraft in Bangalore India. Upon arrival in Bangalore it was noted that  $M^3$  was the last instrument selected for inclusion on the Chandrayaan-1 mission and the first instrument delivered for integration.

[72] In the period through August 2008,  $M^3$  and eleven other instruments were fully integrated and tested with the Chandrayaan-1 spacecraft. In September the fully integrated spacecraft was shipped to the launch site at Sriharikota on the eastern coast of India for integration with the PSLVXL launch vehicle. On the 22nd of October 2008 Chandrayaan-1 was launched through a narrow weather window. The spacecraft was transferred from Earth to lunar orbit and stabilized in the nominal 100 km polar orbit. Early in the mission, thermal anomalies were encountered by Chandrayaan-1 and operation and mission plans were adjusted to accommodate them.  $M^3$  entered instrument checkout in lunar orbit on the 18th of November and acquired a first light image on the 19th of November 2008. Based on successful checkout a flexible plan was developed to acquire a full  $M^3$  data set of the Moon in Global Mode as well as a significant fraction of the lunar surface in high resolution Target Mode. As a result of the extraordinary efforts of the Chandrayaan-1 mission team under challenging operational conditions,  $M^3$  acquired measurement over 95% of the lunar surface in Global Mode. The Chandrayaan-1 space mission concluded abruptly on

the 29th of August 2009 following loss of communications with the spacecraft. The Chandrayaan-1 science mission continued with ongoing analysis of measurements returned by M<sup>3</sup> and the full suite of Chandrayaan-1 science payloads.

[73] During the time of active data acquisition and following the conclusion of the Chandrayaan-1 operational mission, the M<sup>3</sup> science mission focused on the calibration and validation of the M<sup>3</sup> imaging spectrometer measurements. A science data calibration processing pipeline was developed to convert downlinked CCSDS packet to Level 0 data and then to Level 1b. Level 1b provides M<sup>3</sup> measurements with spectral, radiometric, and spatial calibration as well as with full orthographic location and observation conditions. As part of the science validation effort, the M<sup>3</sup> science team has actively pursued the designated science goals and objectives of the M<sup>3</sup> Discovery Mission. In conjunction with this science team validation activity, a focused on-orbit calibration validation effort has been pursued. A series of key subsets of the full M<sup>3</sup> data set have been used to validate the spectral, radiometric, spatial and uniformity characteristics of the M<sup>3</sup> imaging spectrometer. Of particular importance was the validation of the M<sup>3</sup> imaging spectrometer requirement of >90% spectral cross-track uniformity and >90% spectral IFOV uniformity. With a unique Earth-look data set, the spectral cross-track uniformity was initially validated. A set of high latitude M<sup>3</sup> measurements were used to validate the imaging spectrometer spectral IFOV uniformity. As with Galileo NIMS, Cassini VIMS, EO-1 Hyperion, CRISM and other space imaging spectrometers, the on-orbit calibration assessments and validation efforts for M<sup>3</sup> will continue into the future.

[74] The M<sup>3</sup> calibrated imaging spectrometer data set is the first of its kind for the Moon and available for a wide range of scientific analyses and investigations. The M<sup>3</sup> imaging spectrometer instrument used many new elements to achieve this science measurement capability of high uniformity and high SNR as well as low mass, low power, and compact volume. These elements are now available for inclusion in future space imaging spectrometers with comparable science measurement objectives and requirements for new understanding of composition and processes throughout the solar system.

[75] **Acknowledgments.** The authors are deeply grateful to the Indian Space Research Organization for providing this guest opportunity for M<sup>3</sup> to participate in the Chandrayaan-1 mission and the broad support over the course of the mission including contributions for this paper. We also gratefully acknowledge the NASA Discovery Program for supporting M<sup>3</sup> development, implementation and science validation. A portion of this work was carried out at the Jet Propulsion Laboratory/California Institute of Technology, Pasadena, California, under contract with the National Aeronautics and Space Administration.

## References

- Backlund, J., D. Wilson, and R. Muller (2004), Structured-groove phase gratings for control and optimization of the spectral efficiency, in *Diffractive Optics and Micro-Optics, OSA Tech. Digest*, Paper DMB6.
- Berk, A., L. S. Bernstein, G. P. Anderson, P. K. Acharya, D. C. Robertson, J. H. Chetwynd, and S. M. Adler-Golden (1998), MODTRAN cloud and multiple scattering upgrades with application to AVIRIS, *Remote Sens. Environ.*, 65, 367–375, doi:10.1016/S0034-4257(98)00045-5.
- Berk, A., G. P. Anderson, P. K. Acharya, J. H. Chetwynd, L. S. Bernstein, E. P. Shettle, M. W. Matthew, and J. H. Adler-Golden (1999), *MODTRAN 4 Users Manual*, report, Air Force Res. Lab. Space Veh. Dir., Hanscom AFB, Mass.
- Bibring, J. P., et al. (2005), Mars surface diversity as revealed by the OMEGA/Mars Express observations, *Science*, 307(5715), 1576–1581.
- Boardman, J. W., C. M. Pieters, R. O. Green, S. R. Lundein, P. Varanasi, J. Nettles, N. Petro, P. Isaacson, S. Besse, and L. A. Taylor (2011), Measuring moonlight: An overview of the spatial properties, lunar coverage, selenolocation, and related Level 1B products of the Moon Mineralogy Mapper, *J. Geophys. Res.*, 116, E00G14, doi:10.1029/2010JE003730.
- Clark, R. N. (1999), Spectroscopy and principles of spectroscopy, in *Manual of Remote Sensing*, edited by A. Rencz, pp. 3–58, John Wiley, Hoboken, N. J.
- Coradini, A., et al. (1998), VIRTIS: An imaging spectrometer for the ROSETTA mission, *Planet. Space Sci.*, 46(9–10), 1291–1304.
- Goswami, J. N., and M. Annadurai (2008), Chandrayaan-1 mission to the Moon, *Acta Astronaut.*, 63(11–12), 1215–1220.
- Goswami, J. N., and M. Annadurai (2009), Chandrayaan-1: India's first planetary science mission to the moon, *Curr. Sci.*, 96(4), 486–491.
- Green, R. O., et al. (1998), Imaging spectroscopy and the Airborne Visible Infrared Imaging Spectrometer (AVIRIS), *Remote Sens. Environ.*, 65(3), 227–248, doi:10.1016/S0034-4257(98)00064-9.
- Green, R. O., B. E. Pavri and T. G. Chrien (2003), On-orbit radiometric and spectral calibration characteristics of EO-1 Hyperion derived with an underflight of AVIRIS and in situ measurements at Salar de Arizaro, Argentina, *IEEE Trans. Geosci. Remote Sens.*, 41(6), 1194–1203.
- Hunt, G. R., and J. W. Salisbury (1970), Visible and near-infrared spectra of minerals and rocks. I. Silicate minerals, *Mod. Geol.*, 1, 283–300.
- Kieffer, H. H., and R. L. Wildey (1996), Establishing the Moon as a spectral radiance standard, *J. Atmos. Oceanic Technol.*, 13(2), 360–375, doi:10.1175/1520-0426(1996)013<0360:ETMAAS>2.0.CO;2.
- Kumar, A. S. K., A. Roy Chowdhury, A. Banerjee, A. B. Dave, B. N. Sharma, K. J. Shah, K. R. Murali, S. Mehta, S. R. Joshi, and S. S. Sarkar (2009), Hyper spectral imager for lunar mineral mapping in visible and near infrared band, *Curr. Sci.*, 96(4), 496–499.
- Kramer, G. Y., et al. (2011), Newer views of the Moon: Comparing spectra from 1 Clementine and the Moon Mineralogy Mapper, *J. Geophys. Res.*, 116, E00G04, doi:10.1029/2010JE003728.
- Kurucz, R. L. (1995), The solar irradiance by computation, in *Proceedings of the 17th Annual Review of Conference on Atmospheric Transmission Models, PL-TR-95-2060*, vol. 1, edited by G. P. Anderson et al., pp. 333–334, Philips Lab., Geophys. Dir., Hanscom AFB, Mass.
- Maker, P. D., R. E. Muller, and D. W. Wilson (2002), Diffractive optical elements on non-flat substrates using electron beam lithography, U.S. Patent 6480333, Calif. Inst. of Technol., Pasadena, Calif., 12 November.
- McCord, T. B., R. N. Clark, B. R. Hawke, L. A. McFadden, P. Owensby, C. M. Pieters, and J. B. Adams (1981), Moon: Near-infrared spectral reflectance, a first good look, *J. Geophys. Res.*, 86(B11), 10,883–10,892, doi:10.1029/JB086iB11p10883.
- Mouroulis, P., R. O. Green, and T. G. Chrien (2000), Design of pushbroom imaging spectrometers for optimum recovery of spectroscopic and spatial information, *Appl. Opt.*, 39(13), 2210–2220, doi:10.1364/AO.39.002210.
- Mouroulis, P., R. G. Sellar, D. Wilson, J. Shea, and R. O. Green (2007), Optical design of a compact imaging spectrometer for planetary mineralogy, *Opt. Eng.*, 46, 063001, doi:10.1117/1.2749499.
- Murchie, S., et al. (2007), Compact Reconnaissance Imaging Spectrometer for Mars (CRISM) on Mars Reconnaissance Orbiter (MRO), *J. Geophys. Res.*, 112, E05S03, doi:10.1029/2006JE002682.
- Pieters, C. M. (1983), Strength of mineral absorption features in the transmitted component of near-infrared reflected light: First results from RELAB, *J. Geophys. Res.*, 88(B11), 9534–9544, doi:10.1029/JB088iB11p09534.
- Pieters, C. M. (1986), Composition of the lunar highland crust from near-infrared spectroscopy, *Rev. Geophys. Space Phys.*, 24(3), 557–578, doi:10.1029/RG024i003p00557.
- Pieters, C. M. (1993), Compositional diversity and stratigraphy of the lunar crust derived from reflectance spectroscopy, in *Remote Geochemical Analysis: Elemental and Mineralogical Composition*, edited by C. M. Pieters and P. A. J. Englert, pp. 309–339, Cambridge Univ. Press, Cambridge, U. K.
- Pieters, C. M., et al. (2011), Mg-spinel lithology: A new rock type on the lunar farside, *J. Geophys. Res.*, 116, E00G08, doi:10.1029/2010JE003727.
- Rodriguez, J. I., H. Tseng, and B. Zhang (2009), Thermal control system of the Moon Mineralogy Mapper instrument, *SAE Int. J. Aerospace*, 1(1), 376–387.
- Simi, C. G., E. M. Winter, M. M. Williams, and D. C. Driscoll (2001), Compact Airborne Spectral Sensor (COMPASS), *Proc. SPIE Int. Soc. Opt. Eng.*, 4381, 129–136, doi:10.1117/12.437000.

- Simi, C., E. Rieth, and F. Olchowski (2009), The Mapping Reflected-energy Sensor-MaRS: A new level of hyperspectral technology, *Proc. SPIE Int. Soc. Opt. Eng.*, 7457, 3–8, doi:10.1117/12.830098.
- Stone, T. C., and H. H. Kieffer (2002), Absolute irradiance of the Moon for on-orbit calibration, *Proc. SPIE Int. Soc. Opt. Eng.*, 4814, 211–221, doi:10.1117/12.451694.
- Thuillier, G., L. Floyd, T. N. Woods, R. Cebula, E. Hilsenrath, M. Herse, and D. Labs (2004), Solar irradiance reference spectra, in *Solar Variability and its Effect on the Earth's Atmosphere and Climate System*, edited by J. M. Pap et al., pp. 171–194, AGU, Washington, D. C.
- Ungar, S. G., et al. (2003), Overview of the Earth Observing One (EO-1) mission, *IEEE Trans. Geosci. Remote Sens.*, 41(6), 1149–1159.
- Vane, G., A. F. H. Goetz, and J. B. Wellman (1984), Airborne Imaging Spectrometer: A new tool for remote sensing, *IEEE Trans. Geosci. Remote Sens.*, 22(6), 546–549.
- Wilson, D. W., P. D. Maker, R. E. Muller, P. Z. Mouroulis, and J. Backlund (2003), Recent advances in blazed grating fabrication by electron-beam lithography, *Proc. SPIE Int. Soc. Opt. Eng.*, 5173, 115–126.
- M. Annadurai, ISRO Satellite Centre, Bangalore 560 017, India.
- D. Barr, B. Buratti, D. Cate, A. Chatterjee, M. Eastwood, V. Essandoh, S. Geier, T. Glavich, R. Green, R. O. Green, V. Haemmerle, L. Hovland, S. Hyman, T. Koch, K. Lee, S. Lundein, P. Mouroulis, K. Plourde, C. Rachó, J. Rodriguez, G. Sellar, H. Sobel, H. Tseng, G. Vane, P. Varanasi, M. White, and D. Wilson, Jet Propulsion Lab., 4800 Oak Grove Dr., Pasadena, CA 91109, USA. (robert.o.green@jpl.nasa.gov)
- S. Besse, S. McLaughlin, and J. Sunshine, Astronomy Department, University of Maryland, Computer and Space Sciences Bldg., College Park, MD 20742, USA.
- J. Boardman, Analytical Imaging and Geophysics, LLC, 4450 Arapahoe Ave., Ste. 100, Boulder, CO 80305, USA.
- L. Cheek, D. Dhingra, J. Head, P. Isaacson, J. Mustard, J. Nettles, and C. Pieters, Department of Geological Sciences, Brown University, PO Box 1846, 324 Brook St., Providence, RI 02912, USA.
- R. Clark, U.S. Geological Survey, MS 964, PO Box 25046, Denver Federal Center, Denver, CO 80225, USA.
- J. Combe and T. McCord, Bear Fight Center, PO Box 667, 22 Fiddler's Rd., Winthrop, WA 98862, USA.
- J. N. Goswami, Physical Research Laboratory, ISRO, Ahmedabad 380009, India.
- R. Klima, Planetary Exploration Group, Applied Physics Laboratory, Johns Hopkins University, 11100 Johns Hopkins Rd., Laurel, MD 20723, USA.
- G. Kramer, Lunar and Planetary Institute, 3600 Bay Area Blvd., Houston, TX 77058-1113, USA.
- A. S. K. Kumar, Space Applications Centre, ISRO, Ahmedabad 380015, India.
- E. Malaret, ACT Corp., 112 Elden St., Ste. K, Herndon, VA 20170 MD, USA.
- N. Petro, Planetary Geodynamics Branch, NASA Goddard Space Flight Center, 8800 Greenbelt Rd., Greenbelt, MD 20771, USA.
- C. Runyon, Department of Geology and Environmental Geosciences, College of Charleston, 66 George St., Charleston, SC 29424-0001, USA.
- C. Smith, Spacecraft Systems and Services, ATK, 404 N. Halstead St., Pasadena, CA 91107, USA.
- M. Staid, Planetary Science Institute, 1700 E. Fort Lowell, Ste. 106, Tucson, AZ 85719, USA.
- L. Taylor and K. Thaisen, Planetary Geosciences Institute, Department of Earth and Planetary Sciences, University of Tennessee, 306 EPS Bldg., 1412 Circle Dr., Knoxville, TN 37996, USA.
- S. Tompkins, DARPA, 3701 North Fairfax Dr., Arlington, VA 22203-1714, USA.